OPEN ACCESS

Materials Chemistry REVIEW

Multimetallic catalysts for glycerol electrochemical oxidation to value-added products

Shuibo Wang,[1,2] Haocheng Li,[1] Zhongyuan Ma,[1] Yichao Lin,[1,3,*] and Liang Chen[1,3,*]

*Correspondence: yclin@nimte.ac.cn (Y.L.); chenliang@nimte.ac.cn (L.C.)

Received: September 16, 2025; Accepted: May 12, 2026; Published Online: May 12, 2026; https://doi.org/10.59717/j.xinn-mater.2026.100219

© 2026 The Author(s). This is an open access article under the CC BY license (https://creativecommons.org/licenses/by/4.0/).

GRAPHICAL ABSTRACT

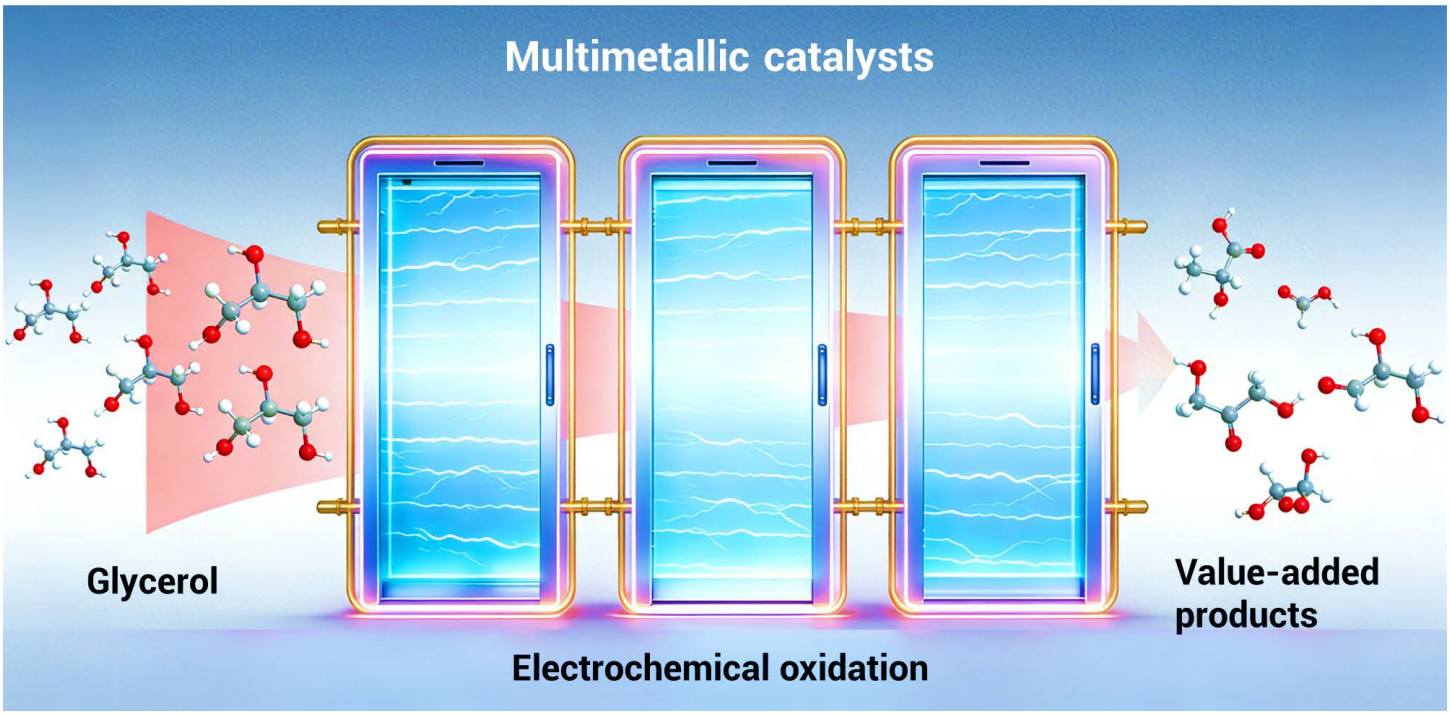

PUBLIC SUMMARY

- Reviews advancements in multimetallic catalysts for glycerol electrochemical oxidation to various products.
- Discusses catalyst design strategies aimed at to enhance performance.
- Presents challenges and future opportunities in the field of multimetallic catalysts for glycerol electrooxidation.

REVIEW Materials Chemistry

OPEN ACCESS

www.the-innovation.org/the-innovation-materials

Multimetallic catalysts for glycerol electrochemical oxidation to value-added products

Shuibo Wang,[1,2] Haocheng Li,[1] Zhongyuan Ma,[1] Yichao Lin,[1,3,*] and Liang Chen[1,3,*]

[1]Zhejiang Key Laboratory of Advanced Fuel Cells and Electrolyzers Technology, Ningbo Institute of Materials Technology and Engineering, CAS, Ningbo 315201, China

[2]Baima Lake Laboratory, Hangzhou 310053, China

[3]University of the Chinese Academy of Sciences, Beijing 100101, China

*Correspondence: yclin@nimte.ac.cn (Y.L.); chenliang@nimte.ac.cn (L.C.)

Received: September 16, 2025; Accepted: May 12, 2026; Published Online: May 12, 2026; https://doi.org/10.59717/j.xinn-mater.2026.100219

© 2026 The Author(s). This is an open access article under the CC BY license (https://creativecommons.org/licenses/by/4.0/).

Citation: Wang S., Li H., Ma Z., et al. (2026). Multimetallic catalysts for glycerol electrochemical oxidation to value-added products. *The Innovation Materials* **4**:100219.

Glycerol is a major byproduct of biodiesel production and has become a biomass-derived platform chemical. The glycerol electrooxidation reaction (GEOR) offers a promising route for valorizing this abundant byproduct under mild conditions, simultaneously mitigating biomass resources and utilizing renewable electricity. However, while GEOR aligns with sustainable and low-carbon development, it faces significant challenges, including sluggish reaction kinetics and complex reaction pathways, which result in low activity and poor selectivity for the desired product. Multimetallic electrocatalysts have emerged as highly efficient materials for glycerol electrooxidation, attracting significant research attention. In this review, we provide an overview of multimetallic electrocatalysts for GEOR. Specifically, we first introduce the reaction networks of GEOR, alongside the intrinsic properties of metallic active sites that govern these processes. We then highlight advanced catalyst design strategies tailored to enhance GEOR performance for the production of specific C1-C3 value-added products. Based on structural-activity correlation, the practical significance of designing site-specific active centers to target distinct products is emphasized. Finally, we outline outstanding challenges and future research priorities that must be addressed to advance the field of GEOR, spanning innovations in catalyst design, advances in reaction engineering, and deeper fundamental mechanistic understanding.

INTRODUCTION

Glycerol sources

The urgent need to enhance energy security and achieve carbon neutrality necessitates exploring alternative renewable energy sources. According to the International Energy Outlook, the deployment of renewable energy is projected to increase substantially by 2050.[1] Non-food biomass—a sustainable and abundant resource—offers a technically feasible and economically viable solution.[2,3] Industrial biodiesel production utilizes cost-effective alkaline transesterification of waste oils, avoiding expensive feedstocks from earlier generations.[4-7] Furthermore, biodiesel, a renewable fuel with high energy density,[8-10] reduces greenhouse gas emissions by approximately 35% versus petroleum diesel.[4,11-13] Since 1991, global non-food biodiesel production has risen steadily,[14-16] with an estimated annual growth rate of 17.5% projected for the period 2023–2027.[17]

However, glycerol, as an abundant and low-value byproduct,[18,19] constitutes approximately 10% of total output. Including glycerol from bioethanol synthesis and soap manufacturing, global production reached 3.62 billion liters in 2016.[18] Further glycerol market growth is projected over the next decade, driven by growing biodiesel output and stringent environmental regulations.[20-22] Although glycerol serves functional roles in food, pharmaceuticals, and fine chemicals (e.g., as humectants, stabilizers, and emulsifiers),[23-27] supply drastically exceeds demand, with a market price of approximately $110 per metric ton.

Products of glycerol oxidation

Valorizing waste glycerol into high-value oxidation products has attracted substantial research attention due to its economic, environmental, and sustainability merits. Glycerol serves as a versatile platform molecule for producing diverse valuable chemicals via selective oxidation, with product distribution (especially organic acids and their salts) highly dependent on reaction medium alkalinity. Key oxidation products include: C_3 compounds: 1,3-dihydroxyacetone (DHA, applied in cosmetics and polymers);[28,29] glyceraldehyde (GLAD, applied in pharmaceuticals);[30,31] glyceric acid or glycerate (GLA, applied in surfactants, polymers);[32-34] hydroxypyruvic acid (applied in pharmaceutical synthesis);[35,36] tartronic acid or tartronate (TA, applied in emulsifiers and pharmaceuticals);[37-39] ketomalonic acid (applied in inorganic synthon);[40] lactic acid or lactate (LA, applied in biopolymers and solvents).[41] C_2 compounds: Glycolic acid or glycolate (GLCA, applied in food additives and polymers);[42,43] oxalic acid or oxalate (OA, applied in decolorizers and skincare).[44] C_1 compound: Formic acid or formate (FA, applied in fuel cells and preservatives).[45-47]

Advantages and challenges of GEOR

Waste glycerol valorization methods include biological conversion, thermocatalytic oxidation, and electrocatalytic strategies (electroreduction and GEOR). Biological routes often suffer from low yields and separation issues, while thermocatalysis typically requires energy-intensive setups, hazardous oxidants (e.g., permanganate, chromic acid),[48] elevated temperatures/pressures, and stringent safety protocols.[49] In contrast, electrocatalytic strategies operate under atmospheric pressure/temperature using renewable electricity (wind, solar, etc.). Glycerol electroreduction—an underexplored viable valorization route to products like 1,3-/1,2-propanediol,[50,51] acetol and propanols[52,53] —differs from GEOR in single reactors. GEOR occurs at anode, involving dehydrogenation and oxygen atom incorporation to produce C_1-C_3 oxygenates, and typically requires a membrane). Conversely, GEOR takes place at the cathode via hydrogenation processes, generally preserves C-C backbone, and can be conducted without a membrane. Compared to glycerol electroreduction, GEOR has garnered extensive research attention yet poses greater challenges for the selective conversion to diverse target products.

The development of GEOR is challenged by sluggish reaction kinetics and poor selectivity, yielding ≥10 distinct products (Figure 1). Product diversity stems from competing factors: glycerol hydroxyl groups co-oxidation, adsorbate configuration variety, and C-C/C-H cleavage.[54,55] Extensive research focuses on multifunctional electrocatalysts to enhance GEOR activity/selectivity. Among these, multimetallic systems (comprising two or more metals) represent a particularly promising class. Synthesized by incorporating secondary metals into primary metal matrices, these electrocatalysts surmount the inherent limitations of monometallic counterparts via synergies from structural engineering (alloys, core-shell, heterostructures, etc), tailoring geometric/electronic properties to optimize selective GEOR toward value-added C_{1-3} products.[56] Leveraging surface strain, electronic modulation, and ensemble effects,[57-59] they promote intermediate adsorption and lower activation barriers; engineered defect sites (steps, kinks, and vacancies),[60,61] 3d metal alloying,[62] and porous/2D structures further enhance catalytic activity, mitigate poisoning, and accelerate mass transfer. Therefore, multimetallic electrocatalysts enable significant improvements in selective GEOR through the modulation of crystallographic structures, morphologies, compositions, and electronic states, etc.

This review aims to elucidate the features and advantages of multimetallic electrocatalysts, delving into the structure-performance relationships of GEOR, and seeking trends in the design of multimetallic electrocatalysts toward specific value-added compounds (Figure 2). Initial discussion addresses fundamental GEOR pathways and mechanisms. Section 2 then analyzes intrinsic product selectivity and glycerol adsorption configurations

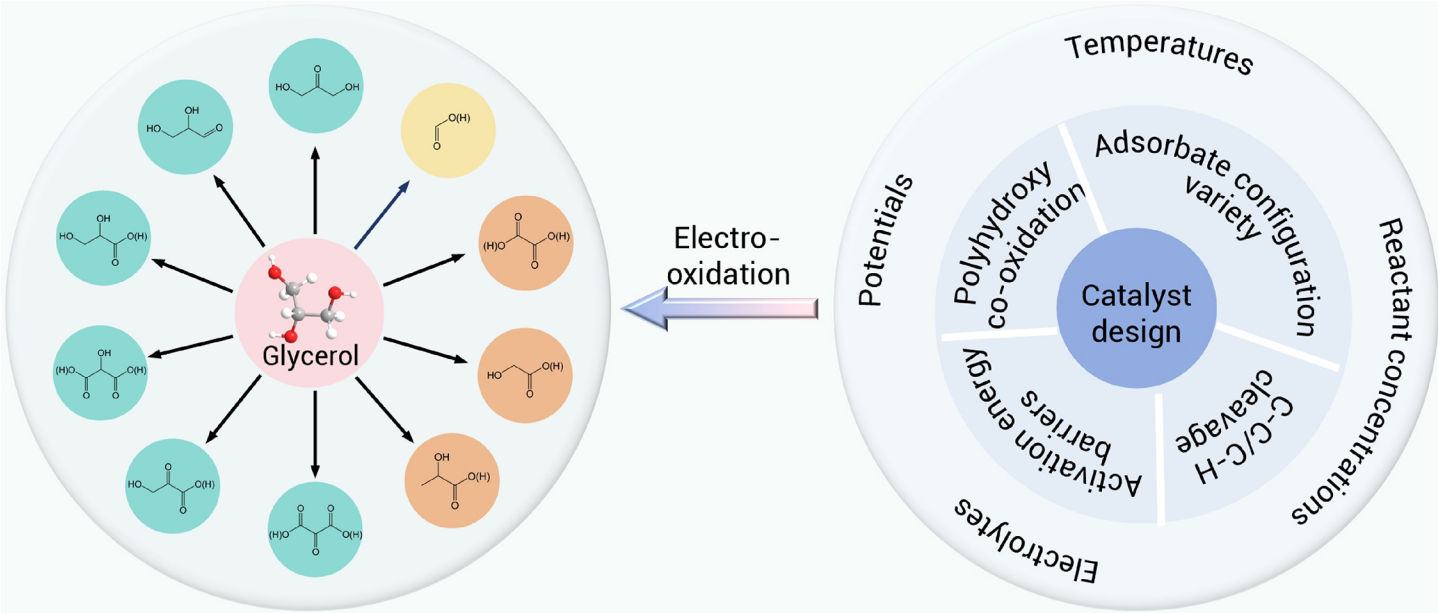

Figure 1. Various value-added products from GEOR depending on reaction conditions and catalyst properties.

on distinct metal sites. Subsequent sections 3-5 detail tailored multimetallic strategies for selectively producing C_3, C_2, and C_1 products respectively, incorporating insights on active-site customization for pathway-specific optimization. The stability bottlenecks, coupled cathodic reaction, and product separation methods are systematically deliberated as critical avenues for future advancement. To guide the rational design of high-performance electrocatalysts, a multimetallic local reaction microenvironment model is proposed. Finally, concluding perspectives provide an overview of future GEOR research trajectories. This work ultimately provides foundational principles for rationally designed metallic electrocatalysts in organic electrosynthetic applications.

REACTION PATHWAYS OF GEOR

GEOR proceeds via a complex pathway, yielding a diverse array of C_1-C_3 products. Figure 3 provides a comprehensive summary of the reaction pathways involved in GEOR. Initially, glycerol undergoes oxidation to form either GLAD or DHA, with a preference determined by the oxidation of hydroxyl groups at specific positions. Notably, under alkaline conditions, glycerol exhibits a pronounced preference for oxidation to GLAD over DHA. Subsequently, GLAD or DHA undergoes further oxidation to generate C_3-C_1 products, as C-C bond cleavage and subsequent oxidation cannot be suppressed at some catalyst active sites. Finally, FA could undergo further electrooxidation to CO_2 under these conditions.

Beyond catalyst intrinsic properties, operational conditions exert a profound impact on the activity, selectivity, and stability of GEOR systems. Key parameters include temperature, applied potential, electrolyte pH, cation/anion species, and glycerol concentration. Elevating temperature enhances the kinetic rate of GEOR by providing sufficient activation energy to overcome reaction barriers. However, temperature also exerts a metal-specific effect on catalyst stability: for instance, elevated temperatures promote the dissolution of Pt while inhibiting Ru leaching, highlighting the need for temperature optimization tailored to catalyst composition.[63] Applied potential and electrolyte pH are two interrelated parameters that jointly regulate product distribution and reaction kinetics. The increasing potential and pH will affect the distribution of products and accelerate the reaction kinetics. Higher potentials facilitate C-C bond cleavage, increasing the yields of C_1 and C_2 species and, in some cases, leading to exclusive formation of C_1 products or CO_2.[34] Similarly, increasing KOH concentration (a common strategy to adjust pH and electrolyte conductivity) not only enhances ionic conductivity but also promotes C-C bond cleavage, further tuning product selectivity.[64] The relationship between glycerol concentration and current density follows a volcano trend, governed by the diffusion coefficient of glycerol. At low

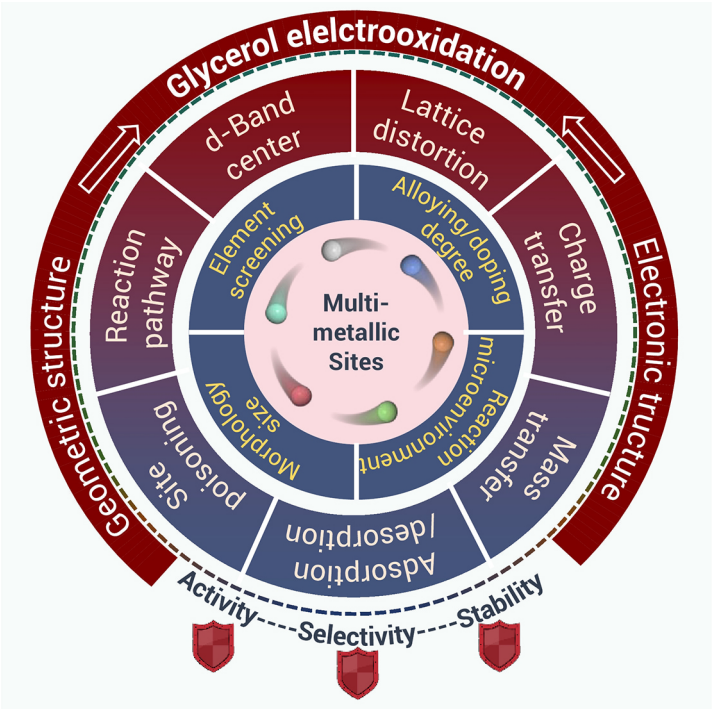

Figure 2. Multimetallic electrocatalysts for GEOR.

concentrations, current density is limited by reactant diffusion to active sites, while excess glycerol may lead to competitive adsorption with reaction intermediates or block mass transfer, resulting in a decline in performance.[64,65] Furthermore, the electrolyte cations influence the reaction on surface through OH_{ad}-$M^+(H_2O)_x$ clusters (M+ = Li^+, Na^+, K^+), formed via non-covalent interaction between hydrated alkali metal cations and adsorbed OH. For example, increasing cation radius can promote activity of catalyst.[66] Cation species also affect formation rate and oxidation rate of adsorbed CO (a catalytic poison) and its potential. While all systems exhibit analogous voltammetry profiles and CO_{ad} intensity signatures for bridge-bonded/multiply bonded CO_{ad} and linearly bonded CO_{ad}, distinct cation-induced discrepancies emerge in the in situ surface-enhanced infrared absorption spectroscopy in the attenuated total reflectance mode (ATR-SEIRA spectra, Figures 4A–C).[67] Specifically, complete oxidation of CO_{ad} is achieved at 1.0 V vs. RHE in LiOH,

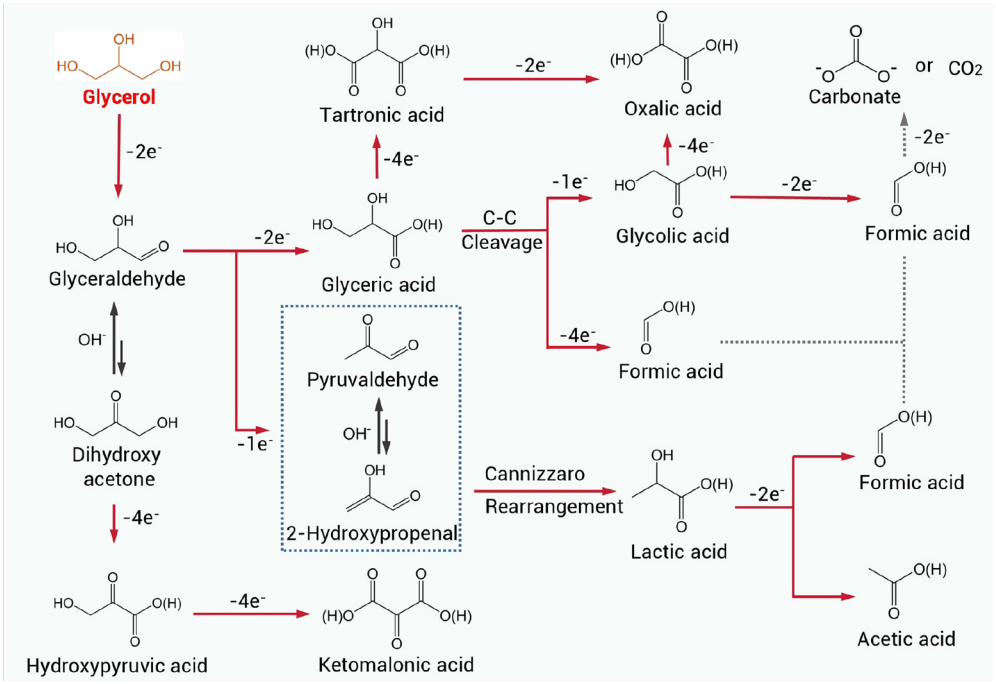

Figure 3. Reaction pathways of GEOR.

whereas a higher potential of 1.1 V vs. RHE is required for full oxidation in NaOH and KOH electrolytes. This is attributed to cation-dependent stability of oxygenated species and electric filed on the surface.[67] Furthermore, cations can drive structural evolution of catalysts, such as inactive Pt oxide layer formation. Anions, meanwhile, regulate the adsorption behavior of glycerol and its intermediates. For example, Huang et al. demonstrated that borate anions form bis-chelated (1:2) complexes with glycerol by coordinating with its hydroxyl groups.[68] These coordination complex formations were confirmed by capillary zone electrophoresis and ^{11}B NMR spectroscopy (Figure 4D). This temporary protection effect preserves intermediate species such as dihydroxyacetone (DHA) and glyceraldehyde (GLAD), preventing their overoxidation and thus tuning product selectivity. Thus, given the strong dependence of GEOR performance on operational parameters, conditions must be tailored to specific catalyst compositions to achieve targeted production of C_1-C_3 products. Beyond optimizing traditional parameters, innovative operational strategies have been developed to address inherent challenges: pulse potential protocols mitigate catalyst poisoning by periodically desorbing accumulated intermediates (Figure 4E-F),[69,70] while flow reactor designs enhance mass transfer by minimizing concentration gradients at the catalyst surface.

The GEOR pathways can be classified into direct and indirect processes.[71] In the direct pathway, glycerol undergoes direct oxidation at the catalytically active sites (Figure 5A). Multimetallic catalysts exert precise control over like inhibiting cleavage of C–C bonds through the introduction of metallic promoter. For example, our group proposed a high-entropy nanosurface strategy (Figure 5B) that PtCuCoNiMn exhibit excellent activity and high GLA selectivity (75.2%).[34] In situ surface-enhanced Raman spectroscopy (SERS) reveals the formation of surface-enriched oxygenated species following surface activation (Figure 5C). These species play a dual role: they stabilize the exposed Pt active sites by forming a protective interface and suppress the non-targeted production of lactate (a key side product in GEOR). Complementary in situ surface-enhanced attenuated total reflection Fourier-transform infrared spectroscopy (SEATR-FTIR) provides mechanistic clarity into the GEOR pathway, confirming sequential activation, dissociation, and adsorption of the primary –OH group of glycerol. This initial step facilitates the stepwise transformation of glycerol to GLAD and further to GLA (Figure 5D). The introduction of Cu species inhibits the hydroxyl departure of dehydrogenated GLAD and further limit formation of the by-product LA. The promoters of Co, Ni, and Mn can protect the Pt sites from oxidation.[34] In indirect pathway, the deployment of electron shuttle mediators (halides, organic nitroxyl species, and heterogeneous polymeric constructs/active species, etc.) is indispensable for facilitating efficient electron transfer kinetics.[72] These mediators, as dynamic redox couples, undergo reversible oxidation-reduction cycles at the electrode-electrolyte interface to shunt electrons from GEOR to the anode (Figure 5E). The choice of mediator dictates the mechanistic pathway, with halides enabling halogen-based redox shuttling,[73-75] nitroxyl radicals facilitating proton-coupled electron transfer,[75] and polymeric scaffolds providing structural confinement for enhanced shuttle efficiency. Moreover, Mohamed et al. presented that the relation between glycerol concentration and GEOR mechanism (Figure 5F).[76] At low glycerol concentrations, the direct oxidation mechanism prevails, wherein glycerol molecules engage with surface-adsorbed OH^- species at catalytic active sites to initiate dissociative adsorption and subsequent C–H/O–H bond activation.[76] Conversely, at elevated glycerol concentrations, the indirect oxidation pathway becomes dominant, driven by the saturation of metallic adsorption sites with glycerol molecules.[76]

OVERVIEW OF THE CATALYTIC SITES FOR SELECTIVE GEOR

As summarized in Table 1 & Figures 6A-C, an overview of typical metallic electrocatalysts employed in the GEOR for the production of C_1–C_3 products is presented. Precious metallic species (e.g., Pt, Pd, Au) are predominantly utilized for the synthesis of C_2 and C_3 products in GEOR. This preferential application originates from the higher added value of C_2 and C_3 products, which effectively offsets the substantial cost of precious metals. Furthermore, the production of C_3 products necessitates low applied potentials to suppress C-C bond cleavage and rapid reaction kinetics. Consequently, precious metal species with high intrinsic activity constitute the dominant active sites for C_2 and C_3 product generation in GEOR. In contrast, non-precious metallic species, with relatively high activation energy barriers, are primarily employed for the synthesis of formic acid, a C_1 product.

Prior to discussing multimetallic systems, monometallic GEOR catalysts are surveyed to establish baseline catalytic behavior at single-metal active sites. The GEOR is a complex reaction network;[77] for instance, the initial glycerol dehydrogenation step proceeds through two distinct intermediates resulting from cleavage of either a secondary C–H or O–H bond (Figure 6D), while subsequent dehydrogenation leads to five possible intermediates (Figure 6E).[78] Theoretical studies suggest that Ru, Rh, Ir, Ag, and Au exhibit selectivity toward DHA and its derivatives, whereas Pd and Pt demonstrate selectivity for either DHA or GLAD and related derivatives (Figure 6F).[79] Theoretical calculation clarifies the structures of key reaction intermediates and reveals that initial deprotonation steps are thermodynamically downhill ($\Delta G < 0$) for most metallic sites, followed by a sequential second deprotonation step.[79] Experimental observations align with these predictions: Pt catalysts facilitate glycerol oxidation to GLA under alkaline conditions, whereas acidic media promote the formation of GLAD.[80] In contrast, Au achieves significant activity only in alkaline electrolytes, generating GLA, LA, GLCA, and FA. Additionally, steric hindrance and inductive effects play critical roles in governing glycerol adsorption behavior on metal surfaces, influencing both molecular orientation and bond activation pathways.[81] For example, glycerol adsorbs more strongly at low-coordination sites and six-adatom triangular defects on Pt(111) surfaces via permanent-induced dipole interactions, where anionic oxygen atoms coordinate with electron-deficient Pt atoms.[82]

Non-noble metals offer compelling cost advantages for GEOR but face limitations including insufficient activity and low selectivity for C_3 products. Nickel-based catalysts facilitate C-C bond cleavage while mitigating poisoning effects,[83] yet their complex electronic configurations generate diverse GEOR products.[84] Mohamed et al. revealed a dynamic Ni speciation cycle (β-

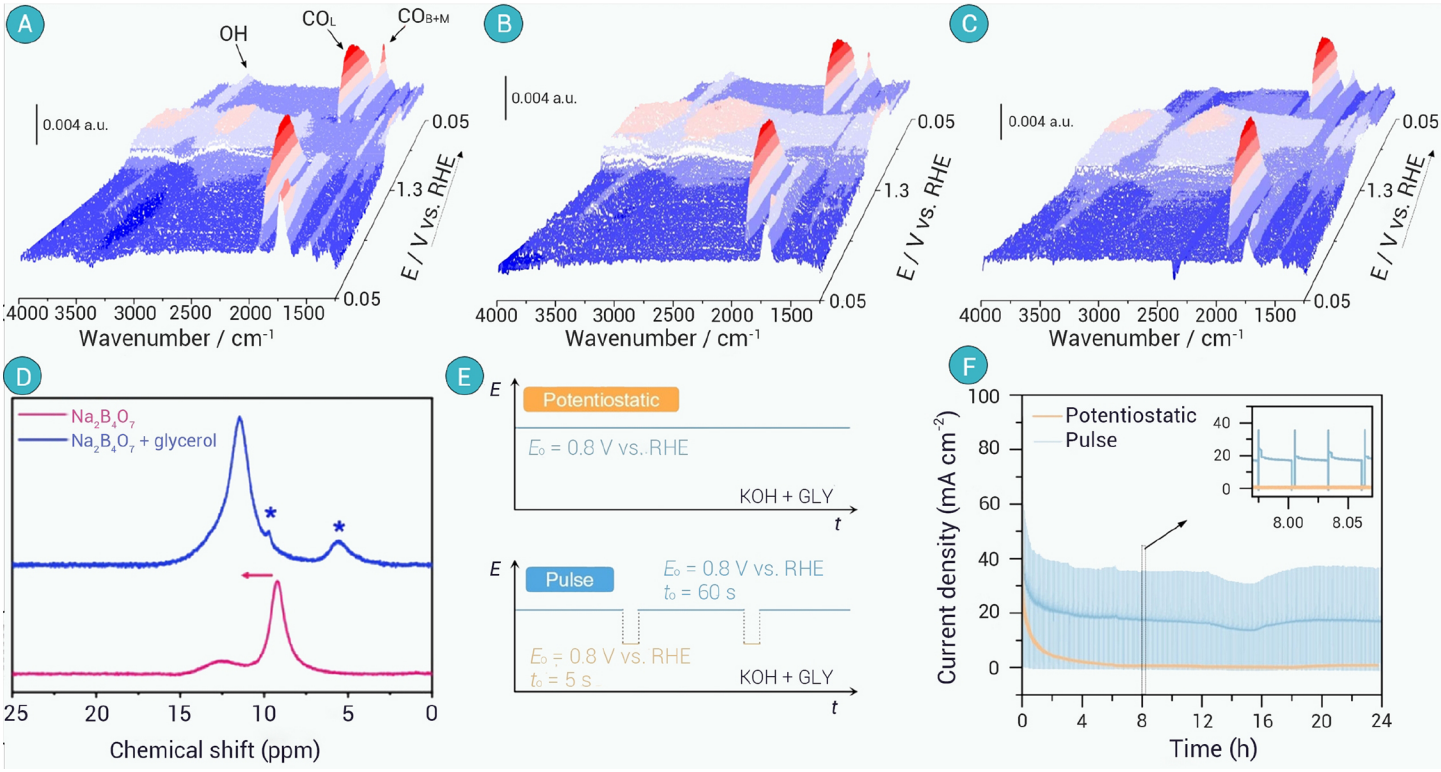

Figure 4. The effect of reaction conditions on GEOR (A-C) time-resolved ATR-SEIRA spectral series recorded during CV of GEOR. CV measurements were performed at a scan rate of 10 mV s^{-1} over the potential range 0.05-1.30 V vs. RHE in electrolytes containing 0.5 M KOH (A), NaOH (B), or LiOH (C), each supplemented with 0.1 M glycerol.[67] This article is open access. Reprinted from Yukuhiro et al. with permission. (D) ^{11}B NMR spectra of 0.1 M borax aqueous solution in the absence and presence of 0.1 M glycerol (* denotes the characteristic signal of borate-glycerol coordination complexes).[68] Copyright 2021, American Chemical Society. (E) schematic illustration of GEOR on Pd-based electrodes with distinct electrolytic strategies.[70] Copyright 2024, John Wiley and Sons. (F) I-t curves of GEOR om Pd over 24 h by asymmetric pulse potential and potentiostatic strategy (Inset: magnified view of the i–t curves highlighting electrode response during the long-term stability test).[70] Copyright 2024, John Wiley and Sons.

NiOOH/β-Ni(OH)$_2$) in 1 M KOH that mediates glycerol oxidation via an indirect electron-transfer mechanism (Figures 7A-B).[85] Ni oxide nanoparticles demonstrate superior GEOR activity and OA yield compared to Fe, Mn, and Co oxides.[44] Cu-based electrocatalysts have been engineered for GEOR toward FA.[86] Cu(II) species with reduced electron cloud density, generated during GEOR, facilitate the adsorption of OH^- on the catalyst surface to form Cu(II)-OH_{ads}, which concurrently enhances glycerol oxidation kinetics (Figure 7C).[87] Furthermore, engineered Cu electrocatalysts facilitate glycerol adsorption.[86] The Cu (II)/Cu (III) redox cycle establishes a dynamic shuttle mechanism that steers selective product formation. However, Fan et al. identified that inadequate oxygen anion deintercalation capacity can impede overall catalytic efficiency in the application of copper-based catalysts.[88] Cobalt-based catalysts also exhibit enhanced electrochemical stability, reduced interfacial impedance, accelerated electron transfer kinetics, and improved oxidation rates, owing to their inherent C–C cleavage ability and stable glycerol adsorption configurations.[89,90] Mn and Bi species have been shown to effectively inhibit C–C bond cleavage during glycerol conversion.[91,92] McKenna et al. reported a glyceric acid selectivity of 82% using $MnSb_2O_6$.[91] Complementary studies by Li et al. reveal glycerol limits lattice oxygen mobility and inhibits MnO_2 dissolution.[93] Bi species further modulate electronic structures of active sites and facilitate secondary hydroxyl group oxidation. DFT calculations demonstrate that introducing proximal Bi atoms significantly weakens the surface adsorption affinity toward all C_3 products, driven by enhanced electrostatic repulsion (Figure 7D).[94] This effect stems from Bi-induced electronic modulation: Bi's p-orbital characteristics and charge redistribution alter the surface electrostatic environment (Figure 7E).[92,94] Additionally, Pb and Fe-based catalysts have been applied in GEOR for the production of mesoxalate and FA, respectively.[95,96] The d-band center of active sites can be precisely tuned via metallic site interactions (e.g., alloying, d-p orbital hybridization), thereby optimizing adsorption thermodynamics and promoting product desorption.

SELECTIVE GEOR: C_3 PRODUCTS

The C_3 products derived from glycerol electrooxidation are of particular interest due to their higher economic value, compared with C_2 and C_1 products. C_3 oxidation products include DHA, GLAD, GLA, TA, and ketomalonic acid, with an increase on the extent of oxidation. However, the inherent susceptibility of glycerol to C-C bond cleavage during this process leads to undesirable deep oxidation, generating lower-value products and significantly diminishing C_3 selectivity. Currently, controlling the reaction pathway to achieve selective oxidation towards specific high-value C_3 products, while suppressing C-C bond scission, remains a critical challenge in the catalytic valorization of glycerol into high-value chemicals.

DHA

DHA, the initial oxidation product of glycerol, represents one of the most valuable derivatives from glycerol oxidation due to its extensive applications in pharmaceutical intermediates, functional additives, food, and cosmetics. Its commercial significance is underscored by a cost approximately 600 times greater than that of glycerol.[97-99] Selective oxidation of the secondary hydroxyl group of glycerol to DHA is a critical yet challenging transformation, primarily hindered by the competitive oxidation of glycerol's three hydroxyl groups. Competing pathways lead to GLAD formation and subsequent over-oxidation to GLCA, resulting in suboptimal DHA selectivity.[100]

The incorporation of Bi as a promoter metal has proven effective in enhancing selectivity toward DHA. Bi atoms selectively suppress the oxidation pathways of primary alcohol groups within the reaction system.[101,102] Kimura et al. were the first to demonstrate that the introduction of Bi into Pt-based catalysts significantly improves DHA selectivity.[103] However, conventional Bi-modified catalysts suffer from inherent limitations: Bi nanoparticles can block Pt active sites, and Bi species are prone to leaching under reaction conditions due to strong chelation with carbonyl intermediates. To address these issues, Leng et al. developed a Pt/Bi@NC architecture, which incorporates N-stabilized Bi single atoms adjacent to Pt nanoparticles.[100] This design minimizes the coverage of Bi on active Pt sites, thereby improving noble

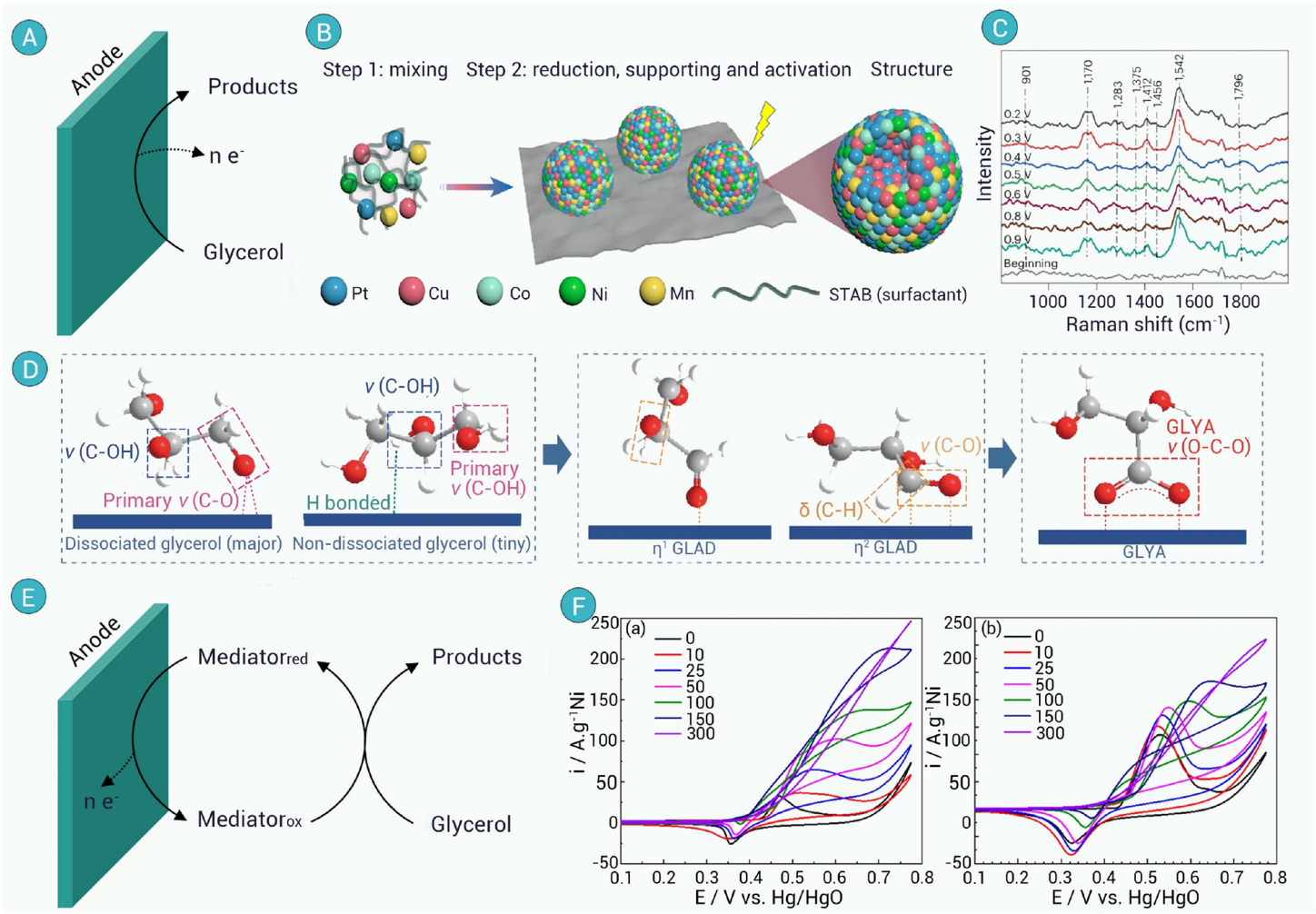

Figure 5. Direct and indirect GEOR processes (A) diagram of direct process; (B) synthesis procedure and TEM image of nanoscale high-entropy surface strategy.[34] Copyright 2025, Springer Nature. (C) In situ SERS of PtCuCoNiMn-EC at multiple applied potentials at 1 M KOH and 0.1 M glycerol.[34] Copyright 2025, Springer Nature. (D) Proposed GEOR mechanism on PtCuCoNiMn-EC.[34] (E) Diagram of indirect process. (F) Cyclic voltammogram (CV) profiles of (a) Ni, (b) $Ni_{95}Pd_5$ measured in 1 M KOH electrolyte containing x mM glycerol, with the potential held at 0.62 V vs. Hg/HgO.[76] Copyright 2019, American Chemical Society

metal utilization while promoting selective secondary alcohol oxidation and achieving high DHA yield. In addition to noble metal based electrocatalysts, non-precious alternatives, such as CuO or MnO_2, exhibit considerable DHA selectivity as well. Chiang et al. reported that CuO catalyzes secondary hydroxyl oxidation under mild alkaline conditions, attaining high DHA selectivity albeit at a low current density of ~3 mA cm^{-2}.[104] Zhao et al. engineered a MnO_2-CuO/CF electrode that achieves high DHA selectivity at reduced applied potentials.[105] The interpenetrating architecture of MnO_2 lamellae and CuO dendritic structures accelerates electron transfer and mass transport of reactants and products. Synergistic interactions within this system enhance glycerol adsorption while suppressing that of DHA. These effects collectively reduce the overpotential and boost the selectivity toward DHA.[105] In situ Raman spectroscopy enables real-time tracking of dynamic surface evolutions of catalysts under reaction conditions. Zhao et al. utilized this technique to visualize the in-situ formation of a stable MnO_2-containing surface structure during catalysis (Figure 8A).[105] Such findings underscore that heteroatom incorporation tunes the electronic structure of active sites and modulates the adsorption/activation of reaction intermediates, a key strategy for optimizing catalytic performance via coordination environment engineering.

Efficient catalysts for GEOR-driven DHA synthesis commonly feature tailored active site electronic structure and strong substrate adsorption specificity. Their structural design is primarily shaped by the heteroatom effect, crystal plane and defect formation, which collectively govern catalytic performance. Currently, mainstream strategies for DHA synthesis via GEOR include introducing Bi and Pb heteroatoms for structural modulation, or utilizing oxidized species (like MnO_2) to tailor the electronic structure of active sites and the adsorption configuration of glycerol. A persistent challenge in this process is insufficient catalytic activity, characterized by low current density.

GLAD/GLA

GLAD is a key chemical intermediate widely used in the pharmaceutical, chemical, and food industries. GLA and its derivatives, which function as biologically active food additives, command a market price of approximately \$30 mol^{-1}, with global demand reaching 1.445 million tonnes.[106] The strategic design of adsorption sites plays a critical role in determining the adsorption modes and capacities of reactants and intermediates, thereby steering product distribution. For instance, Kim et al. employed atomic layer deposition to coat SnO_2 on commercial Pt/C (Figure 8B).[107] The resulting SnO_2-Pt interface enhanced the adsorption of reaction intermediates while inhibiting the sintering of Pt nanoparticles in acidic media, thereby altering the GEOR pathway and significantly improving GLAD selectivity at comparable conversion levels. Besides catalyst design, it was also reported to enhance GLA selectivity by using pulsed potential to promote glycerol adsorption and facilitating GLA desorption (Figure 8C).[108] Operando in situ FTIR corroborates this mechanism: spectral signatures corresponding to adsorbed aldehyde intermediates (1590 cm^{-1}) exhibit progressive intensification, consistent with site-blocking and catalyst poisoning.[108] In contrast, application of the pulsed potentials induces a marked reduction in these absorption bands. Notably, signals at 1400 cm^{-1} (carboxylate species) and 1588 cm^{-1} (aldehyde species) show pronounced attenuation, directly confirming the suppression of toxic intermediate accumulation. These findings demonstrate that pulsed potential

Table 1. The summary of the performance of metallic electrocatalysts in GEOR for the generation of C1-C3 products.

Electrocatalysts	Electrolytes (M)	Glycerol (M)	Potentials (V vs. RHE)	Current density (mA cm^{-2})	Selectivity (%)	Stability Test (hours)	Turnover frequency	Faradaic efficiency (%)	Ref.
C3 products									
CuO	0.1 M $Na_2B_4O_7$	0.1	2.06	3	~60% DHA	>3	/	/	104
MnO_2-CuO/CF	1 M KOH	0.1	1.3	10.7	60% DHA	30	/	/	105
γ-MnO_2	0.1 M $Na_2B_4O_7$	0.1	1.85	1.9	~50% DHA	/	/	/	147
ALD(SnO_2)– Pt/C (HT)	0.5 M H_2SO_4	0.1	1.136	<1	42%GLAD	/	/	/	107
PtCuCoNiMn	1 M KOH	0.1	0.75	~200	75.2%GLA	210	/	/	34
Pt@G	1 M KOH	0.05	0.7 (pulse)	/	81.8%GLA	/	/	/	108
Ni_xB	1 M KOH	0.1 solketal	1.58	6	77%GLA	>2	/	/	109
Cu_{rich} Cu-$Co(OH)_x(CO_3)_y$	1 M KOH	0.1 solketal	1.5	~10	67%GLA	>4	/	70%	110
Pd_3Bi/C	4 M KOH	1	0.7	~200	~80%TA (30°C)	24	/	/	113
PdCuL/C	2 M KOH	2	0.6	~100	59%TA	48	/	/	114
$Pt_{80}Co_{20}$	2 M KOH	1	0.67	/	72%LA	/	/	/	115
Au/CeO_{2-x}	1 M KOH	0.5	1.5	693.4	81%LA	/	/	/	116
PdZn/TiO_{2-x} NS	1 M KOH	0.5	0.85	~30	~45%LA	15	/	/	117
C2 products									
NiO_x/$MWCNT_s$-O_x	1 M KOH	1	1.5	60	>70%OA	40	/	66%	44
PdAg	4 M KOH	1	/	/	35.9%OA	/	/	/	118
AuPd	0.1 M NaOH	0.1	/	/	~40%GLCA	/	/	/	120
PdFe/rGO	1 M KOH	0.1	0.8	/	45%GLCA	/	/	/	121
$LaFe_{1-x}Co_xO_3$	1 M KOH	1	~1.53	3	13.8%GLCA	48	/	/	122
FA or formic acid									
CuO@$NiBiO_x$	1 M KOH	0.1	1.6	~60	>85%	100	/	79.4%	46
$Ni_{0.9}Au_{0.1}$/C	1 M KOH	0.1	1.04	46	100%	24	/	85%	123
Mo-NiOOH	1 M KOH	0.1	1.51	400	~84.7%	/	/	84.7%	124
CuNiP/CuO_x-V_P Nanoarrays	1 M KOH	0.1	1.75	1000	96.76%	70	/	96.94%	125
NiCoFeRuRe	1 M KOH	0.1	1.133	10	~95.6%	450	/	95.6%	126
Fe-CuO_x/CF	1 M KOH	0.3	1.33	100	95.1%	20	/	87.53%	148
CuNi–$NiVO_x$	1 M KOH	0.1	1.308	10	82.24%	60	5.97 s^{-1}	82.245	127
Pt-in-VGCC	1 M KOH	0.1	/	/	79%	/	/	/	128
Ni_3N/Co_3N-NWs	1 M KOH	0.1	2.01	1000	~94.6%	200	/	94.6%	129
$NiCoO_x$/CN_x-300	1 M KOH	0.1	1.5	~40	~89.7%	48	0.02s^{-1}	87%	133
t-NiCo-MOF	1 M KOH	0.5	1.4	600~730	~90%	/	/	85%	134
NiCo hydroxide	1 M KOH	0.1	1.35	100	94.3%	110	~4.9s^{-1}	~100%	77
CoNiCuMnMo	1 M KOH	0.1	0.55	10	~92.0%	288	31.44h^{-1}	92%	136
N-CoFeP/NF	1 M KOH	0.1	1.38	100	~74%	/	/	74%	137
Ni-Mo-N/CFC	1 M KOH	0.1	~1.5	100	~95.0%	12	/	95.0%	138
$NiCo_2O_4$/NF	1 M KOH	0.1	1.219	10	94.0%	>60	/	93.2%	149
$NiCo_2O_4$/NF	1 M KOH	0.1	1.42	300	~89.9%	200	/	89.9%	150
GDE@AgAu	1 M KOH	0.1	/	/	66%	/	/	/	151

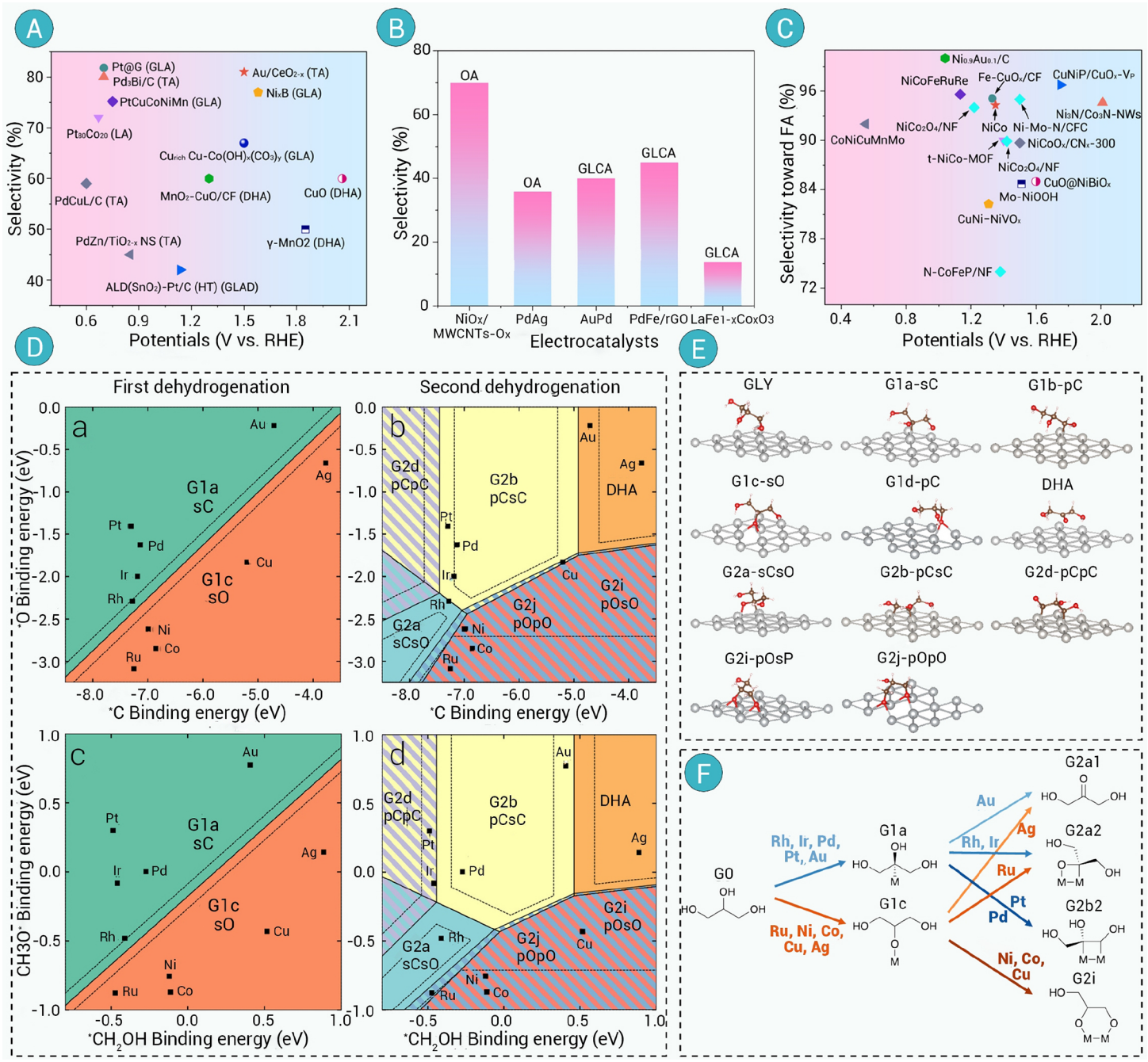

Figure 6. The intrinsic property of various metallic sites for glycerol electrooxidation (A-C) Comparison of the GEOR performance of various electrocatalysts in terms of (A) C_3 product, (B) C_2 product, and (C) FA generation. (D) Selectivity for first-dehydrogenated and second-dehydrogenated intermediates of glycerol as a function of the binding energy of O* and *C (a, b) and of $*CH_2OH$ and CH_3O* (c, d).[78] This article is open access. Reprinted from Valter et al. with permission. (E) Glycerol intermediate structures.[78] This article is open access. (F) Thermodynamically favorable routes (blue color denotes routes starting with carbon deprotonation and orange denotes those starting with oxygen deprotonation).[79] Copyright 2020, American Chemical Society.

regulation enables precise control over the local reaction environment, thereby steering reaction pathways at distinct active sites.

Alternatively, Andronescu et al. introduced an approach involving the condensation of glycerol with acetone to form solketal, a mono-alcohol that mitigates catalyst deactivation and suppresses C-C cleavage. Subsequent electrooxidation of solketal achieved high selectivity toward GLA.[109,110] In another study, a CoNiFeCu multimetallic catalyst was shown to enhance GLA synthesis, achieving a Faradaic efficiency of 40%, while simultaneously inhibiting Cu precipitation (Figure 8D).[111] Duan et al. established a volcano-type relationship between glycerol oxidation activity, hydroxide adsorption free energy (ΔG_{OH}), and glycerol adsorption free energy ($\Delta G*_{ads}$), with Au_3Pd/Au_3Ag alloys exhibiting optimal performance (Figure 8E).[112] Dopant-Au d-orbital coupling upshifts the alloy's d-band center vs. Au. This d-band elevation indicates Fermi-level d-electrons engage more actively in glycerol adsorption. Furthermore, the oxidation state and structural configuration of metal sites are crucial in regulating C-C cleavage. For example, compared with MnO_x (featuring Mn^{4+} in adjacent sites), $MnSb_2O_6$ (with isolated Mn^{2+} sites) significantly suppresses C-C bond scission, resulting in 82% selectivity toward GLA and higher yields of C_3 products.[91]

Efficient GEOR electrocatalysts (targeting GLAD/GLA) exhibit more diverse design strategies than those of DHA, encompassing doping, alloying and pulsed potential modulation. Their core functions include accelerating GLAD/GLA desorption, activating glycerol dehydrogenation, optimizing hydroxyl/glycerol adsorption energies, and enabling rapid active-site regeneration. High-performance catalysts share features: tailored active-site electronic structure and strong substrate affinity without over-adsorption. We

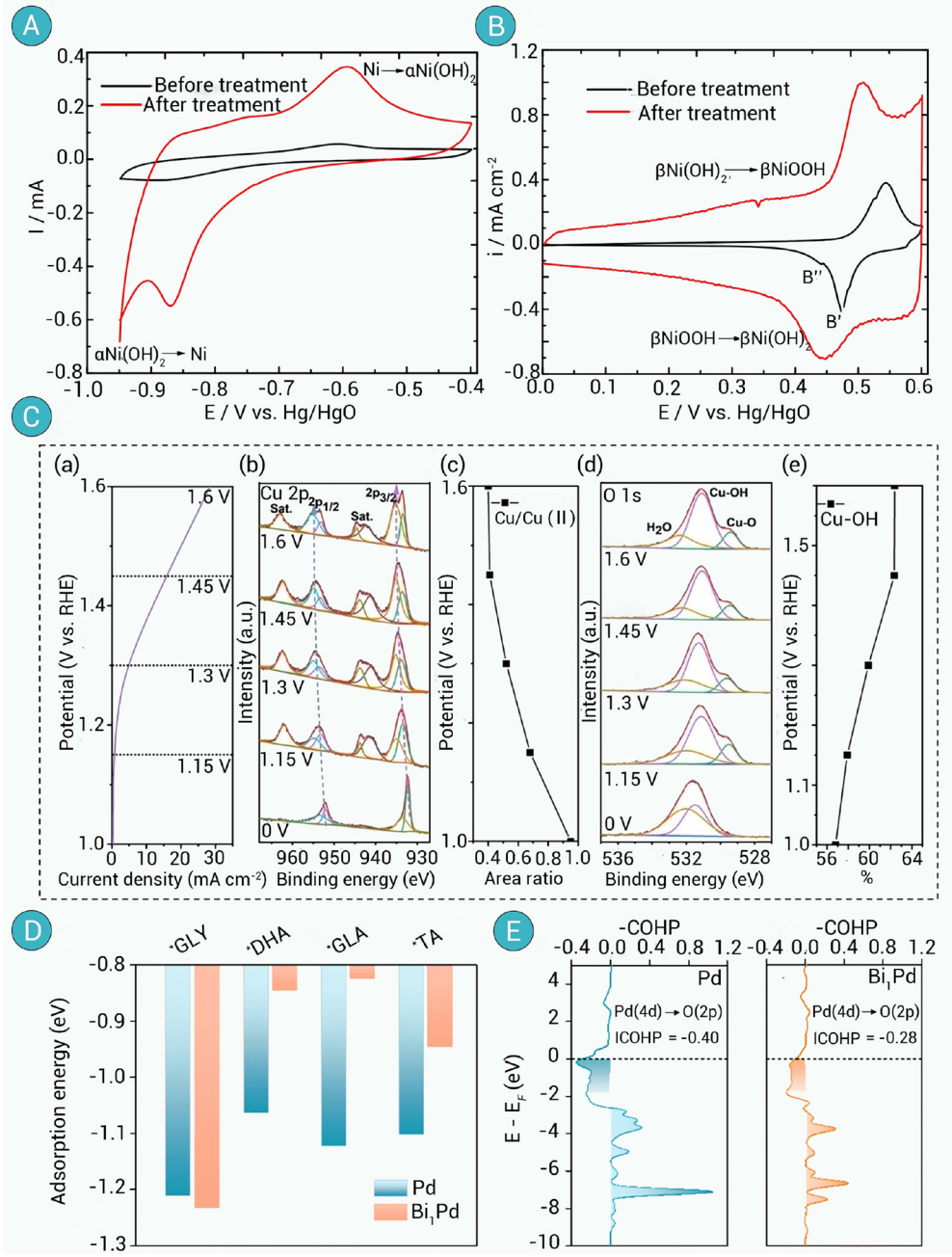

Figure 7. Non-noble metal-based electrocatalysts (A-B) CV profiles of Ni electrocatalyst in 1 M KOH with 50 mV s^{-1} before and after treatment, respectively.[85] Copyright 2017, Elsevier. (C) Ex situ-derived surface analysis of the Cu-CuS/BM catalyst: (a) LSV curve of Cu-CuS/BM, (b) ex situ XPS analysis of Cu 2p of Cu-CuS/BM after LSV tests of GEOR at cutoff potentials of 0, 1.15, 1.3, 1.45, and 1.6 V, (c) Cu^0/Cu^{2+} peak area ratio derived from Cu 2p XPS spectra, (d) ex situ XPS analysis of O 1s of Cu-CuS/BM after LSV tests of GEOR, (e) peak area percentage of surface-adsorbed hydroxyl oxygen, summarized from O 1s XPS.[87] Copyright 2022, American Chemical Society. (D) Adsorption energies of glycerol, DHA, GLA and TA on Bi_1Pd or Pd.[94] (E) Integrated COHP values between the O atom of adsorbed GLA and the Pd atom in Bi_1Pd or pristine Pd.[94] Copyright 2024, Royal Society of Chemistry.

propose that entropy modulation and d-band center tuning synergistically endow electrocatalysts with high selectivity and activity for glycerol-to-GLAD/GLA oxidation, while preserving structural integrity.

Other C3 products

TA, LA, and ketomalonic acid can also be obtained through selective GEOR. Although these oxidized products have received relatively less attention as target products in previous studies, they possess high added value and find applications in diverse fields, including polymers, emulsifiers, inorganic synthons, and solvents. Herein are some design strategies for catalysts to selectively yield TA, LA, and ketomalonic acid. For example: (i) Modification of catalytic sites by second metal species (such as doping and alloying).[113-115] (ii) Tuning the local microenvironment of the reaction.[116] (iii) Regulation of the nanostructure of support (involving aspects like defects, strong support-metal interaction, and enrichment of adsorption sites).[117] PdCu alloy nanoparticles (NPs) stabilized by a secondary diamine ligand display enhanced TA selectivity due to the Pd-Cu synergistic effect and possess structural stability thanks to the protection provided by the ligand.[114] Huang et al. introduced the CeO_{2-x} Lewis acid component to suppress local acidification and augment the surface concentration of OH^-.[116] The accelerated diffusion of OH^- and the increased OH^- concentration led to an LA selectivity of 81.2% when using Au/CeO_{2-x}.[116] In a catalyst, multiple of the above strategies can be combined to bring about a more significant improvement in GEOR performance. Nevertheless, further efforts are still needed for the separation and purification of C_3 products.

SELECTIVE GEOR: C_2 PRODUCTS

The primary high-value-added C_2 products derived from glycerol electrooxidation are GLCA and OA. However, C-C bond cleavage and subsequent deep oxidation inevitably generate C_1 byproducts, predominantly FA (formic acid). OA exhibits inherent stability under typical electrocatalytic conditions, functioning as a terminal oxidation product due to the inertness of its carboxylic acid groups.[44,118] Similarly, further oxidation of GLCA is kinetically hindered, requiring significantly elevated potentials; this barrier arises from the protective effect of the adjacent carboxylate/carboxylic acid group ($-COO^-$/-COOH) on the reactive hydroxyl moiety.[118]

OA

Within alkaline media, Pd sites exhibit exceptional capability for glycerol deprotonation, while Ag species promote C-C bond cleavage and oxidation of aldehyde-containing intermediates.[118] Illustrating this synergy, Neeva et al. synthesized PdAg bimetallic alloy NPs with tunable Pd/Ag ratios, demonstrating that Ag incorporation significantly increases the proportion of metallic Pd^0 species.[118] These PdAg NPs exhibit markedly enhanced GEOR activity, OA selectivity, and faradaic efficiency, coupled with a low onset potential in 1 M KOH containing 0.1 M glycerol. Surface-exposed Pd^0 sites were identified as critical centers for glycerol deprotonation. Although intrinsically inactive for GEOR, Ag sites within the bimetallic structure facilitate C-C bond cleavage in intermediates (e.g., mesoxalate and TA) adsorbed on adjacent Pd sites, thereby steering the pathway towards C_2 (OA) production.

Beyond random alloys, ordered intermetallic structures can further enhance performance. Wang et al. demonstrated the nanostructure of intermetallic PtBi hexagonal nanoplates (Figure 9A), which exhibit superior GEOR activity, stability, and high OA selectivity under identical alkaline conditions.[119] In these nanoplates, Pt exists predominantly in the metallic state, while surface Bi species are oxidized; the strong electron interaction between Bi and Pt drives electron transfer from Bi to Pt sites. This mass activity reached 3.2 times that of commercial Pt/C. Although alloying with Bi enhances structural stability, trace Bi dissolution remains observable. Mechanistic studies

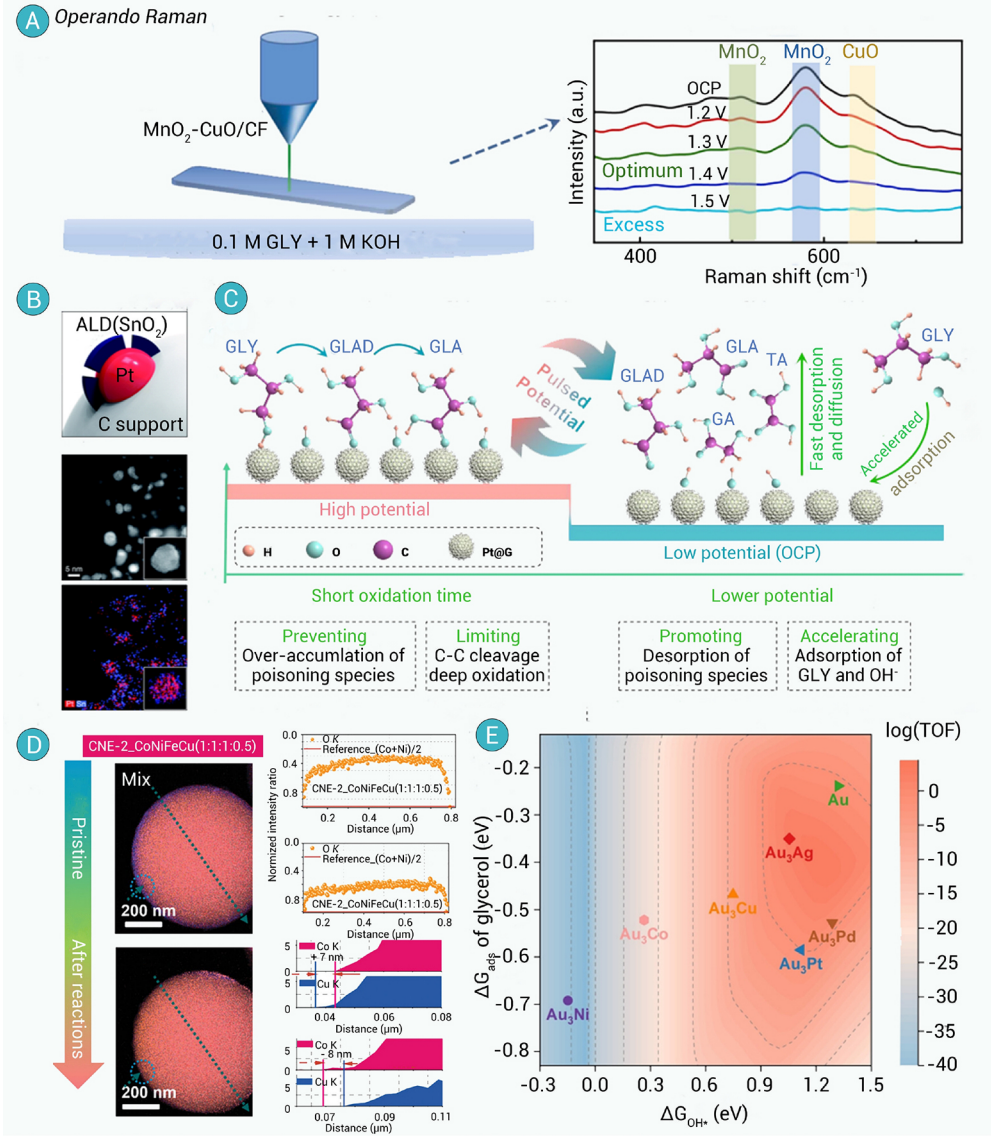

Figure 8. Strategies for enhancing C_3 product selectivity (A) Operando Raman spectra recorded at various applied potentials.[105] Copyright 2024, Elsevier. (B) Schematic illustration, HAADF-STEM images and the corresponding EDS elemental mapping images for 300ALD(SnO_2)-Pt/C (HT).[107] Copyright 2020, Royal Society of Chemistry. (C) Reaction pathway diagram for of GEOR using pulsed potentials. GLY glycerol, GLAD glyceraldehyde, GLA glyceric acid, TA tartronic acid, GA glycolic acid.[108] This article is open access. Reprinted from Chen et al. with permission. (D) Overlay EDX mapping images (Co, Ni, Fe, Cu, C, O) of CoNiFeCu (1:1:1:0.5) nanoassemblies before (up) and after (down) 5 CV cycles of OER, normalized line scan curve (align with the arrow in EDX mappings) for Cu and O of CoNiFeCu (1:1:1:0.5) nanoassemblies before (up) and after (down) 5 CV cycles OER and 8 CV cycles solketal electrooxidation, and parallel line scan curves (marked by circle in EDX mappings) illustrating Co and Cu distributions in CoNiFeCu (1:1:1:0.5) nanoassemblies before (up) and after (down) 5 CV cycles OER and 8 CV cycles solketal electrooxidation.[111] This article is open access. Reprinted from Zhang et al. with permission. (E) Theoretical TOF (in s^{-1}) for GEOR at 1.4 V vs. RHE, plotted on a logarithmic scale.[112] Copyright 2024, John Wiley and Sons.

(Figure 9B) suggest that Bi suppresses C-C bond cleavage in glycerol and intermediates compared to pure Pt, directing selectivity towards C_2 products (OA). In situ FTIR, as presented in Figure 9B, captures the characteristic absorption bands (labeled A–H) corresponding to glycerol and its oxidation products, enabling direct tracking of reaction pathways on catalyst surfaces.[119] A prominent feature emerges in the spectral region associated with the O–C–O stretching vibration of OA at 1308 cm^{-1}: the intensity of this band increases monotonically with increasing applied potential. More notably, the O–C–O band intensity for OA is substantially higher on the PtBi alloy than on monometallic Pt. This dual observation confirms two key phenomena: OA is a kinetically stable product under the reaction conditions, and the PtBi catalyst exhibits enhanced selectivity toward OA formation relative to Pt. A second diagnostic band at 1980 cm^{-1}, attributed to linearly adsorbed carbon monoxide (CO: a typical poisoning intermediate derived from C–C bond cleavage) provides critical mechanistic insight. This CO feature is clearly distinguishable on monometallic Pt but is entirely absent from the FTIR spectrum of PtBi. The selective suppression of CO adsorption on PtBi directly indicates that the alloy structure effectively inhibits the cleavage of C-C bonds in glycerol, a detrimental pathway that limits both activity and selectivity in Pt-based catalysis.

Collectively, these in situ FTIR results underscore the structural advantage of the alloy strategy: by preserving the C–C bond integrity of glycerol and promoting the formation of stable OA, alloy strategy overcomes the inherent limitations of monometallic Pt catalysts in biomass-derived alcohol oxidation reactions. These observations underscore the critical need for precise control over the composition ratio and spatial distribution of electrocatalysts. Efficient catalysts for such reactions typically share high active-site accessibility, modulated electronic structure, and strong substrate affinity to boost selectivity and activity. For GEOR to OA, alloying strategies offer a viable route to enhance the electron cloud density and metallic-state content of catalysts, thereby improving OA selectivity. This catalyst structure design is primarily shaped by active-site utilization efficiency, dopant stability, or the electronic interaction between alloy components.

GLCA

Yaovi et al. reported the synthesis of carbon-supported AuPt and AuPd nanoparticles (NPs) via a bromide anion exchange method.[120] These bimetallic Au-based electrocatalysts exhibited a GEOR selectivity of 40% toward GLCA in 0.1 M NaOH containing 0.1 M glycerol. In a related study, Andrea et al. designed PdFe NPs with a Fe-enriched surface, demonstrating that the incorporation of Fe into the Pd lattice weakens Pd–Pd bonding and reduces the proportion of metallic Pd^0 species.[121] To gain deeper mechanistic insights into the electrocatalytic kinetics of these nanostructured catalysts, electrochemical impedance spectroscopy (EIS) measurements were performed in the kinetic-dominated potential region. Fitting the EIS data with a well-established equivalent circuit model (inset in Figure 9C) revealed distinct charge transfer behaviors between the PdFe alloy and monometallic Pd.[121] Specifically, the PdFe alloy exhibited a substantially smaller charge transfer resistance compared to pure Pd (Figure 9C), reflecting accelerated electron transfer kinetics at the PdFe interface, a phenomenon likely originating from the electronic modulation and lattice strain effects induced by Fe alloying. Such kinetic superiority validates the efficacy of alloying strategies in optimizing both thermodynamic and kinetic aspects of electrocatalytic reactions.

The electrocatalytic performance was evaluated for the tested nanostructures in the kinetic region, that is, a low potential range of 546-746 mV vs. RHE. Through surface segregation analysis, they further revealed that positioning Fe in the first subsurface layer of PdFe NPs yields the most stable configuration, minimizing the high surface energy of Fe and alleviating elastic strain caused by lattice mismatch (Figure 9D). This PdFe nanostructure exhibited a 2.8-fold increase in mass activity compared to pure Pd, with GLCA being the dominant GEOR product (~45%). The enhancement is attributed to the synergistic interaction between Pd and subsurface-stabilized Fe. This interaction optimizes glycerol adsorption behavior and acceler-

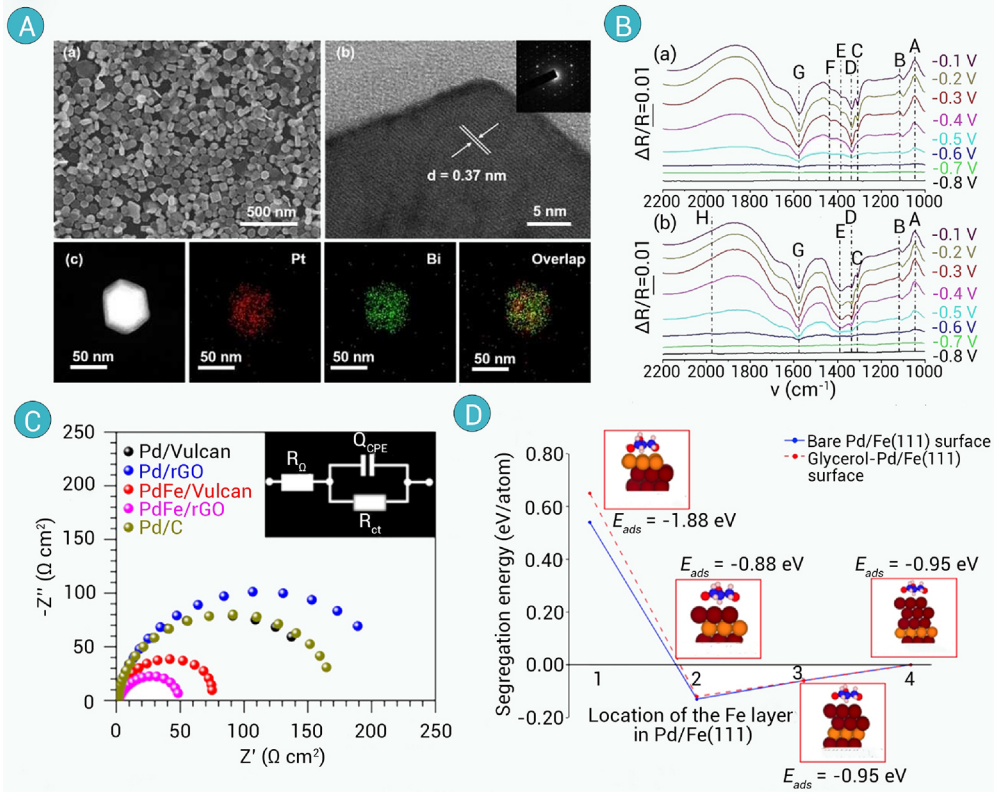

Figure 9. Strategies to enhance GEOR performance for producing C_2 products (A) HAADF and STEM-EDS mapping images of PdAg/CNT.[119] Copyright 2020, John Wiley and Sons. (B) In situ FTIR spectra of glycerol oxidation on (a) PtBi/C and (b) Pt/C catalysts in aqueous electrolyte containing 1 M KOH and 0.1 M glycerol.[119] Copyright 2020, John Wiley and Sons. (C) EIS of GEOR on PdFe catalysts at 0.646 V vs. RHE.[121] Copyright 2021, American Chemical Society. (D) Evolution of the segregation energies (E_{seg} eV/Fe atom) of one-layer Fe from the Pd "bulk" (the fourth layer of the slab) to the first surface layer: DFT-D3 was calculated in the absence or presence of one adsorbed glycerol molecule.[121] Copyright 2021, American Chemical Society.

ates reaction kinetics through electronic and structural modifications. Multimetallic oxides provide another avenue for designing multifunctional active sites and interfaces capable of facilitating cascade reactions in glycerol oxidation. For instance, $LaFe_{0.31}Co_{0.69}O_3$, a perovskite-type oxide (ABO_3), exhibits the lowest GEOR onset potential (1.6 V vs. RHE) among Fe/Co-based perovskites, surpassing other stoichiometric variants.[122] However, $LaFe_{0.72}Co_{0.28}O_3$ achieves the highest GLCA selectivity (14.0%) in 1 M KOH with 1 M glycerol, indicating a trade-off between catalytic activity and product selectivity in GEOR systems. Such a trade-off underscores the necessity of tailoring catalyst composition to match targeted application requirements: whether prioritizing activity for energy conversion or selectivity for value-added chemical synthesis.

For GEOR toward GLCA, the dominant strategy involves alloying to enhance metallic state content of sites and tailor lattice strain. A key distinction from GEOR targeting OA resides in the selection of additive metals. Efficient catalysts for such reactions commonly feature well-defined active sites, strong substrate adsorption, and facile charge transfer properties to obtain electronic modulation, reaction pathway preferences, and the balance between stability and active site accessibility under electrochemical conditions. Further study of non-precious-metal-based perovskites or high-entropy materials hold promise for introducing diverse functional sites to advance this field.

SELECTIVE GEOR: C_1 PRODUCTS

FA is the primary value-added C_1 product through the complete cleavage of C–C bonds in glycerol. A major challenge, however, is suppressing the overoxidation of FA to CO_2, which significantly reduces the selectivity and Faradaic efficiency of the process. To tackle this issue, multimetallic electrocatalysts—particularly those based on non-noble metals—have been developed to improve FA production via GEOR. An optimal surface concentration of OH^- promotes GEOR kinetics, while high bulk concentrations of KOH help suppress the formation of CO_2/CO_3^{2-}, thereby enhancing FA selectivity.

Nickel-based catalysts are highly effective for C–C bond cleavage in the GEOR. The mechanism typically initiates with the phase transformation of β-$Ni(OH)_2$ to the active β-NiOOH. A key strategy to enhance this inherent activity involves modifying the electronic structure, such as through shifts in the d-band center, often achieved via surface segregation in bimetallic systems. For example, Mohamed et al. demonstrated that a $Ni_{0.9}Au_{0.1}$/C electrocatalyst achieves 100% FA selectivity at 1.55 V vs. RHE, with a low onset potential of 0.12 V vs. Hg/HgO.[123] Mohamed et al. indicated the possibility of an Au-core Ni-shell structure which optimized the GEOR performance by modifying the electronic properties of Ni sites.[123] In situ FTIR observed obvious absorption band at ~1350 cm^{-1} corresponds to symmetric (O–C–O) stretching of formate (Figure 10A). Further performance gains are realized through anion leaching and heteroatom doping. Wang et al. developed an anion leaching strategy where MoO_4^{2-} species leach from a $NiMoO_4$ precursor to create Mo-doped NiOOH. During cyclic voltammetry activation, this process increases the Ni^{3+}/Ni^{2+} ratio to accelerate GEOR kinetics, while Mo doping promotes C-C cleavage and suppresses the oxygen evolution reaction (OER).[124] In situ Raman provides direct spectroscopic evidence for the leaching of Mo species, concurrent with the structural reconstruction of $NiMoO_4$ into NiOOH during GEOR. As the electrochemical process proceeds, the two characteristic Raman peaks assigned to NiOOH gradually intensify to dominate the spectral profile, while Mo-associated vibrational bands diminish to negligible intensities (Figures 10B-C).[124] The underlying catalytic mechanism follows a well-defined redox cycle: Ni(II) species within the precursor undergo electrochemical oxidation to form the active NiOOH phase, which then mediates the chemical oxidation of glycerol via its own reduction to nickel $Ni(OH)_2$. This heteroatom-modulated electronic effect likely tunes the d-band filling of Ni active sites, optimizing the adsorption/desorption dynamics of glycerol intermediates and facilitating the critical C-C bond cleavage step for formate formation.

Structural engineering also plays a critical role. Zheng et al. fabricated hierarchically structured nickel phosphide porous nanoarrays with phosphorus vacancies via a glycol-mediated solvothermal method.[125] Doping with Cu induced the aggregation of Cu nanoparticles (Figure 10D), resulting in a superaerophobic-hydrophilic nanostructure that enhances glycerol adsorption/oxidation and product desorption. This synergistic effect achieved a high current density of 1 A cm^{-2}, and FA selectivity of 96.76% at 1.75 V vs. RHE.[125] In addition, Ru- and Re-doped NiCoFe transition metal alloys exhibit exceptional stability (> 450 hours in Figure 11B).[126] Ru facilitates the generation of M^{3+}-OOH active sites for GEOR (Figure 10E), while Re suppresses OER kinetics and mitigates FA overoxidation.

Complementary to heteroatom doping, heterostructure engineering creates interfaces with strong electronic interactions, which optimize charge transfer and the adsorption/desorption energetics of glycerol, its intermediates, and FA. This strategy significantly enhances the density of exposed active sites for efficient C-C cleavage. For example, a CuNi-$NiVO_4$ heterostructure achieves an ultralow potential of 1.308 V vs. RHE at 10 mA cm^{-2} and 82.24% FA selectivity at 1.467 V vs. RHE. This performance is driven by strong interfacial electronic coupling that promotes glycerol and hydroxyl adsorption while facilitating FA desorption (Figure 11A).[127] The critical role of well-defined interfaces is further highlighted by Pt nanosheets engineered for confinement, which demonstrate exceptional efficiency for C-C bond cleavage and

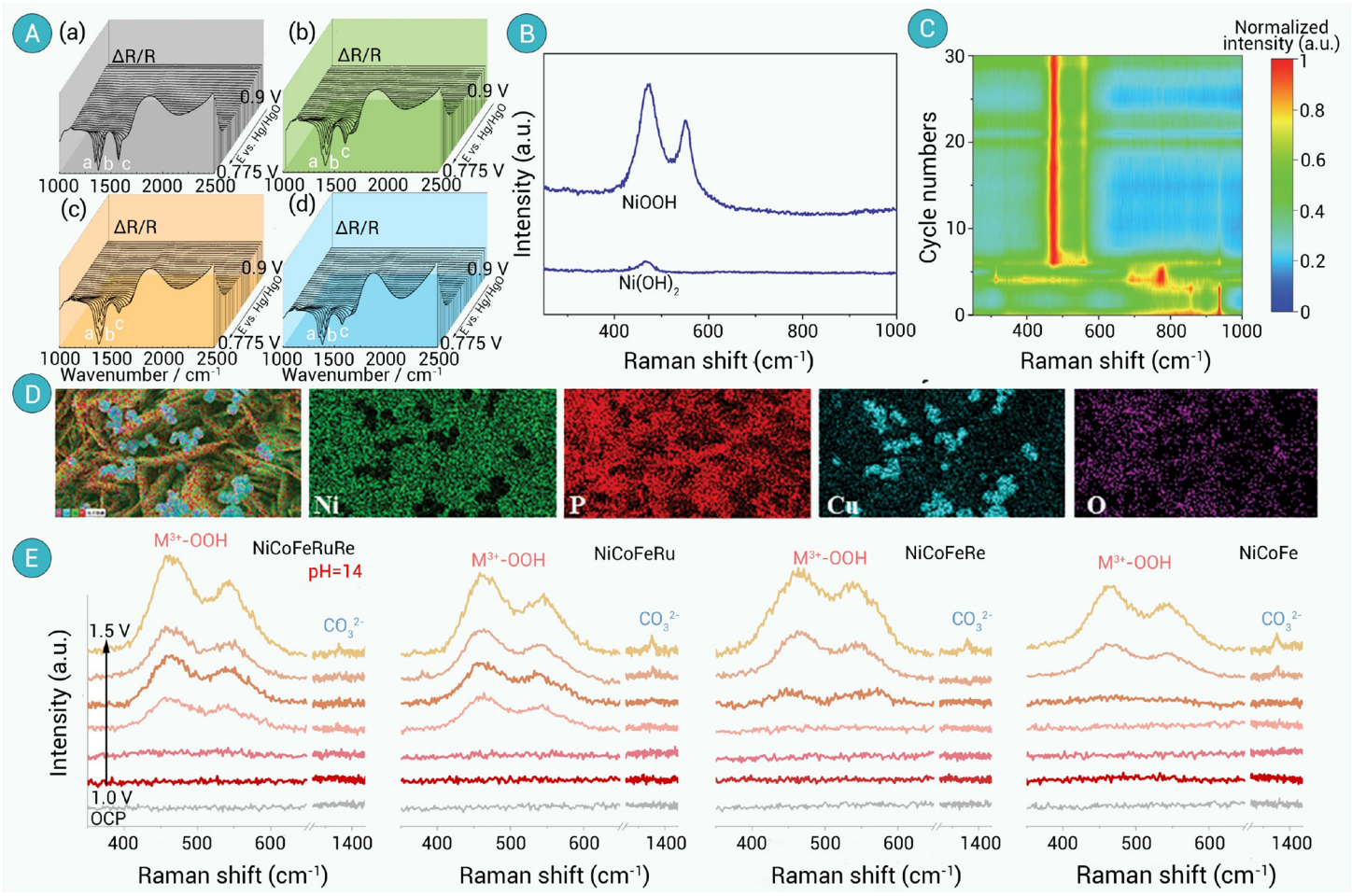

Figure 10. Self-supported electrodes for GEOR performance to produce C_1 products (A) Infrared spectra acquired during GEOR over (a) Ni/C, (b) $Ni_{0.8}Pd_{0.2}$/C, (c) $Ni_{0.9}Au_{0.1}$/C, and (d) $Ni_{0.9}Bi_{0.1}$/C catalysts in 1.0 M KOH electrolyte containing 0.1 M glycerol at 293 K.[123] Copyright 2020, American Chemical Society. (B) Ex situ Raman spectra showing characteristic peaks of Ni(OH) (466 cm^{-1}) and NiOOH (474 and 553 cm^{-1}).[124] This article is open access. This article is open access. Reprinted from Wang et al. with permission. (C) In situ Raman spectra monitoring the structural reconstruction from $NiMoO_4$ to Mo-NiOOH in the 30 CV cycles.[124] This article is open access. Reprinted from Wang et al. with permission. (D) Elemental mapping images of CuNiP/CuO_x-V_P nanosheet array electrodes.[125] Copyright 2024, John Wiley and Sons. (E) In situ Raman spectra of NiCoFeRuRe, NiCoFeRe, NiCoFeRu, and NiCoFe in pH 14 electrolytes.[126] Copyright 2025, John Wiley and Sons.

FA production.[128] Similarly, Ni_3N/Co_3N heterointerfaces exhibit a 94.6% Faradaic efficiency for FA at 1.35 V vs. RHE. A flow electrolyzer incorporating this catalyst achieved a high current density of 1 A cm^{-2} at a low cell voltage of 2.01 V, a result of a modulated electron distribution that accelerates GEOR dehydrogenation kinetics (Figure 11C).[129] The Ni_3S_2/NiFe-LDH heterostructure also demonstrates exceptional performance, requiring only 1.37 V vs. RHE to reach 100 mA cm^{-2} while maintaining 90.3% FA selectivity.[130]

Beyond the regulation of active sites, the strategic design of nanoscale morphology plays a crucial role in modulating the catalytic reaction microenvironment. Controlling the architecture of multimetallic electrocatalysts—such as through 1D/2D nanomaterials[131,132] or porous architectures[133]—significantly enhances GEOR performance by optimizing mass transport, exposure of active sites, and electron transfer. For instance, a core-shell CuO@$NiBiO_x$ nanocage achieves 85% FA selectivity with substantial energy savings. In this system, Bi doping enriches surface Ni^{3+} sites, while the CuO core facilitates rapid charge transfer (Figure 11B).[46] In situ Raman spectroscopy provides definitive evidence for the formation of NiOOH, which we identify as the pivotal active site for GEOR and which supports an indirect reaction mechanism. Specifically, upon introduction of glycerol into the system, the characteristic Raman peak of NiOOH diminishes progressively (green spectrum), and vanishes entirely once the oxygen evolution reaction (OER) electrolyte is fully substituted with GEOR electrolyte (red spectrum). Reverting to the OER electrolyte reverses this spectral evolution confirming the reversibility of its generation-consumption cycle (Figure 11D).[46] Similarly, multimetallic layered double hydroxides (LDHs, e.g., NiCo-LDH) exploit favorable geometric effects to enable rapid intermediate transfer, electronic modulation, and synergistic metal interactions, all contributing to enhanced efficiency.[77,134,135] Furthermore, advanced material classes such as high-entropy nanomaterials,[136] transition metal phosphides,[137] and nitrides[138] have emerged as highly promising candidates for efficient GEOR-to-FA conversion. As the most intensively studied product of GEOR, current catalyst design strategies prioritize boosting the intrinsic activity of active sites while preserving high Faraday efficiency for FA formation by strong substrate affinity, and robust stability. Investigation of in-situ generated active sites (e.g., NiOOH) and advancing non-precious metal electrocatalysts are paramount.

STABILITY: A PERVASIVE CHALLENGE IN GEOR

Most research on GEOR have predominantly focused on enhancing catalytic activity and selectivity, while largely overlooked systematically investigating catalyst stability. GEOR deactivation stems from intertwined chemical and structural mechanisms. Primarily, the decay could be attributed to the strong adsorption of reaction intermediates (e.g., CO, aldehydes) onto active sites: these species exhibit sluggish desorption kinetics, not only blocking active centers but also impeding mass transfer within the catalyst layer. The surface of Pt sites was easily poisoned by the adsorption of CO and intermediates.[139] Second, metal leaching is exacerbated under acidic/alkaline electrolytes,[140] resulting in the irreversible loss of active metallic components. For example, Bi species are prone to leaching under reaction conditions due to strong chelation with carbonyl intermediates.[103] Third, oxidation of catalyst sites forms inert oxides, reducing electron conductivity and catalytic activity.[141,142] For instance, Pt species can be gradually oxidized even at small positive potentials (< 0.8 V vs. RHE).[34] Moreover, pH fluctuations

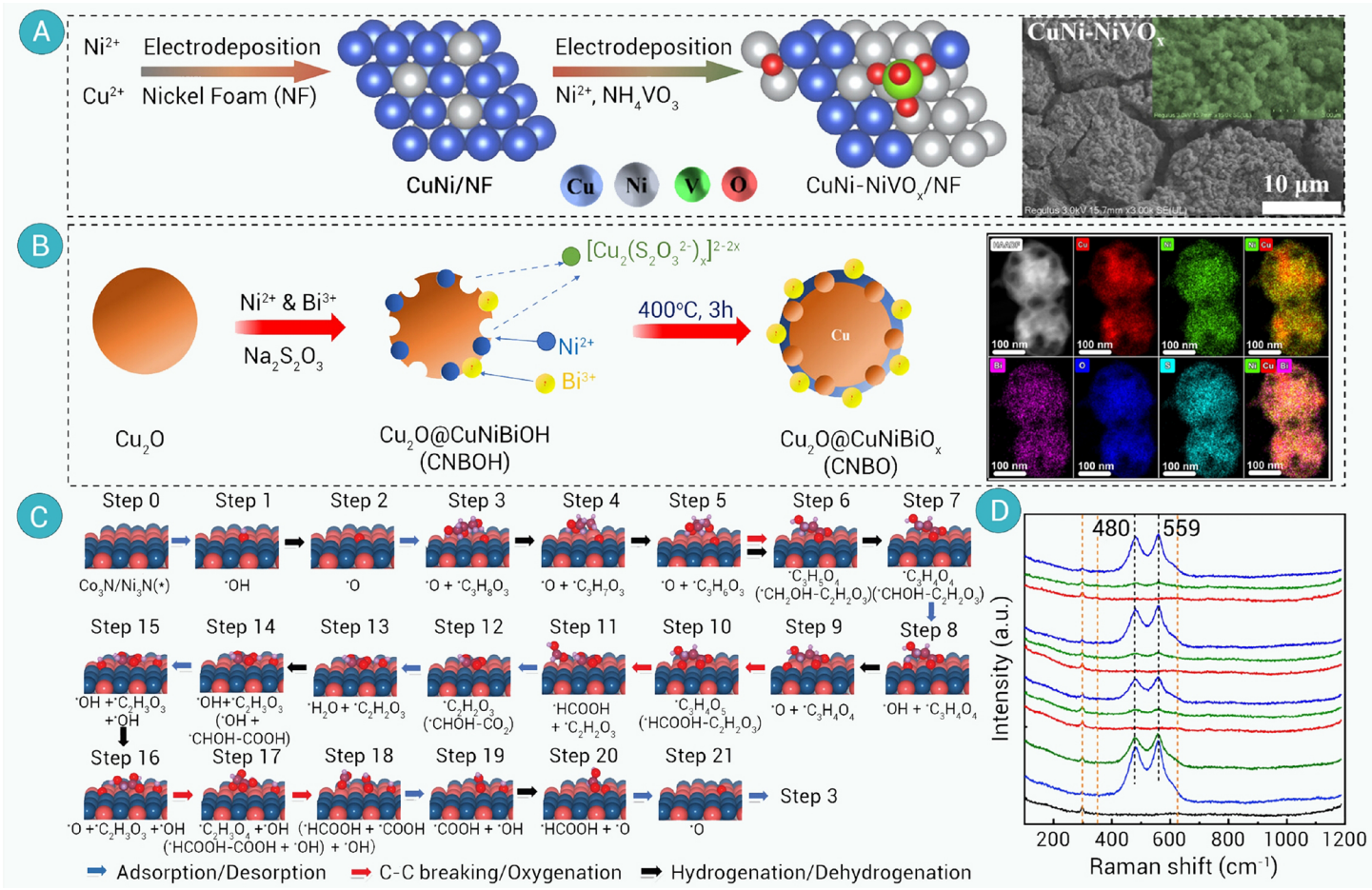

Figure 11. Strategies to enhance GEOR performance for producing C_1 products (A) Synthesis diagram and TEM image of CuNi-$NiVO_x$ on nickel foam.[127] Copyright 2024, American Chemical Society. (B) Schematic illustration for the synthesis of CuO@$NiBiO_x$ and representative EDS elemental mappings of CuO@$NiBiO_x$.[46] This article is open access. Reprinted from Le et al. with permission. (C) Illustration of GEOR pathway and corresponding configurations on Ni_3N/Co_3N heterointerfaces.[129] Copyright 2023, John Wiley and Sons. (D) In situ Raman spectra of CuO@$NiBiO_x$ recorded at different time, obtained under electrochemical conditions in the absence and presence of glycerol.[46] This article is open access. Reprinted from Le et al. with permission.

also alter surface reactivity (e.g., protonation/deprotonation of surface hydroxyl groups), accelerating site deterioration. Additionally, structural agglomeration of nanoparticles at elevated potentials further exacerbates deactivation. Significant agglomeration occurs for Au and Pt NPs, leading to the rapid deactivation of catalyst in GEOR.[142,143]

These deactivation pathways, while distinct in the mechanism, converge to erode active sites or obstruct mass transfer, limiting industrial applicability. Multimetallic catalysts have mitigated these issues leveraging synergistic effects through rational structural engineering: alloy formation tunes electronic structures to suppress oxidation of active sites; phase-segregated domains anchor labile metals against leaching. NiCoFeRuRe high-entropy alloy exhibits exceptional long-term stability due to an accelerated indirect oxidation pathway that minimizes intermediate poisoning,[126] and Co_3O_{4-x}@ZrO_{2-x} heterostructured nanosheets achieved 100 h stability.[144] By explicitly linking each deactivation mode to specific multimetallic synergies, the rational optimization of catalyst structure (e.g., composition, morphology, support interaction) and reaction conditions enables the simultaneous mitigation of multifaceted deactivation pathways, thereby achieving superior GEOR stability. There are also some other methods to alleviate deactivation, e.g. interval chronoamperometry strategy and pulse potential strategies. Nevertheless, the most critical challenges remain the design of stable catalyst structures and the elucidation of deactivation mechanisms. From a theoretical perspective, promising strategies include incorporating corrosion-resistant d^0 metallic species (such as W, Hf, and Ti) to bolster structural integrity, along with controlling the concentration of surface-active species (e.g., hydroxyl groups) to fine-tune intermediate adsorption/desorption and mitigate poisoning.

SUMMARY

In GEOR, the production of distinct C_1-C_3 products necessitates tailored catalyst design strategies and specific metallic active sites. For example, Bi or Pb species enhance C_3 product selectivity by promoting the adsorption of secondary hydroxyl groups, whereas Ni or Co species favor C_2–C_1 product formation due to their inherent C–C bond cleavage capability. To target different products, rational electronic and geometric engineering of active sites and heteroatoms is imperative.

Modification of active sites with second metal species via doping or alloying is a widely adopted approach to regulate site structure, including oxidation state and structural configuration. While this strategy offers advantages such as ease of implementation and diverse compositional flexibility, it remains incremental and heavily reliant on empirical knowledge. Key challenges persist, including potential active site blocking and uncertainties regarding long-term structural stability. Additionally, heterojunction structures can establish interfaces that modulate the adsorption/desorption behavior of glycerol reaction intermediates and optimize mass transfer processes. However, limitations include a restricted number of effective interfaces, sluggish interfacial charge transfer, and difficulties in precisely capturing dynamic phenomena (e.g., interfacial charge transfer) during reaction. In contrast, several highly innovative structural strategies have recently emerged, such as high-entropy materials, single-atom catalysts, and perovskite-based materials, each leveraging unique intrinsic properties to enhance GEOR performance. Tuning the local reaction microenvironment is a disruptive GEOR strategy: support nanostructuring introduces defects, reinforces metal–support interactions, and enriches adsorption sites, enabling maximal active species utilization and optimized kinetics. A paradigmatic case is the immobilization of single-atom sites on support matrices, leveraging their unique electronic/coordination properties to boost catalytic perfor-

mance.

Beyond catalyst design, electrolyte modification (such as the addition of solketal) has been explored to suppress C–C bond cleavage. Despite its critical importance, research on reaction environment regulation in GEOR remains scarce. Innovations in materials science, electrolyte engineering, device design, and artificial intelligence-driven optimization will collectively advance selective GEOR toward industrial viability.

COUPLING CATHODE REACTION AND PRODUCT SEPARATION

GEOR emerges as a powerful alternative anodic process, with accelerated reaction kinetics directly address the fundamental bottleneck of OER. This kinetic advantage translates to a marked enhancement in overall current density, thereby boosting the efficiency of cathodic H_2 production. Beyond its synergy with H_2 generation, the coupling of GEOR with CO_2RR represents an impactful innovation,[46,123] as it enables the formation of a closed carbon loop. Mechanistically, the low onset potential characteristic of GEOR reduces the energy input requirement for CO_2RR. This synergistic interaction not only enhances the energy efficiency of CO_2 conversion but also promotes the selectivity of high-value C_{2+} products by mitigating competing side reactions. In the context of green ammonia synthesis, the GEOR-NO_2RR or GEOR-NRR coupling system offers a game-changing ambient-condition alternative to the energy-intensive Haber-Bosch process.[145,146] Such performance, combined with the potential for simultaneous wastewater remediation through nitrate removal, positions GEOR-NO_3RR as a sustainable and economically viable route for ammonia production. Collectively, these findings establish GEOR as more than a mere alternative to OER; it serves as a transformative catalytic platform integrating renewable energy storage, carbon cycling, and high-value chemical synthesis.

Product separation remains critical for GEOR's industrialization, with strategies tailored to dominant products like formate. For water-soluble carboxylates, electrodialysis efficiently isolates charged species via ion-selective membranes, eliminating solvent waste. Our group also proposed two separation strategies for distinct products after acidification treatment: (i) Cooling crystallization: The resulting acid solution is concentrated by reverse osmosis, followed by cooling crystallization to yield high-purity acids; (ii) Vacuum distillation: The obtained acid solution is concentrated via reverse osmosis and then subjected to vacuum distillation. This strategy enables separation of thermally sensitive chemicals at lower temperatures, mitigating decomposition or polymerization risks of organic acids versus conventional distillation.[34]

MULTIMETALLIC LOCAL REACTION MICROENVIRONMENT MODEL

Catalytic activity, product selectivity, and long-term stability are not independent, which are intrinsic manifestations of interfacial reaction dynamics, collectively determined by catalyst structural features and operational reaction conditions. Specifically, high activity relies on optimal OH^* binding energy at active sites to balance reactant activation and intermediate desorption; high product selectivity demands precise regulation of C-C bond cleavage kinetics and hydroxyl group departure pathways to steer toward target products; and prolonged stability requires robust tolerance to CO poisoning as well as resistance to metal dissolution and surface oxidation. However, there is the trade-off in three metrics (activity, selectivity, and stability): pursuing high activity often necessitates highly oxophilic active sites, yet these lead to metal dissolution, even sacrifice selectivity for valuable oxidation products; Conversely, catalysts designed for high C_3 product selectivity (e.g., those modified with oxyphilic but leaching-prone Bi) often suffer from compromised long-term stability due to the gradual loss of the modifier. To address activity-selectivity-stability trade-off and guide GEOR toward desired pathways, we propose a multimetallic local reaction microenvironment model that tailors the complex reaction network to follow target pathways by precisely engineering three interconnected microenvironments:

(i) Local electronic microenvironment: The local electron density and d-band center of active sites dictate the binding energies of key adsorbates (e.g., OH*, CO, glycerol, and intermediates). Rational alloying or doping of metals enables deliberate tuning of the d-band center of active sites, thereby optimizing the adsorption strength of glycerol and its intermediates to match reaction requirements. Besides, the core-shell strategy utilizes a stable core (like Au) to electronically modify a reactive shell (like Pt), or introduces a thin shell to protect a leaching-prone base metal in the core.

(ii) Local geometric microenvironment: atomic arrangement of surface governs the adsorption of reactants/intermediates, and the spatial orientation of C-C bond cleavage relative to C-O bond activation. For example, isolated active sites (e.g., Au or Pt single atoms) prevent the multi-site binding necessary for C-C bond cleavage, favoring high product selectivity. Controlling the ensemble size of active sites (e.g., specific Pt atomic clusters) can be leveraged to selectively promote C_2 product formation. Besides, electrocatalysts with large, contiguous sites and strong CO-binding energy tend to drive deep oxidation of glycerol toward FA.

(iii) Local electrolyte microenvironment: the types of anions and cations in the electrolyte, the diffusion kinetics of reactants and products at the reaction interface, and the concentrations of surface-active species all regulate GEOR performance. For example, the incorporation of oxyphilic metallic components (e.g., Ni, Cu, Ru, Ag) into multimetallic catalysts: these species enhance local concentration of OH^* in the interfacial microenvironment, thereby accelerating the activation of glycerol molecules and mitigating CO poisoning.

The rational design of multimetallic catalysts for targeted GEOR pathways (toward C_1, C_2, or C_3 products) hinges on the synergistic optimization of these three microenvironments for matching the mechanism requirements of the target reaction pathway and simultaneously mitigating the deactivation of active sites for producing C_1-C_3 products.

CONCLUDING REMARKS AND OUTLOOKS

In this review, we have comprehensively surveyed recent advances in the GEOR using multimetallic catalysts. A systematic analysis of the complex reaction networks and the intrinsic properties of metallic active sites that govern GEOR pathways has been presented. We highlighted innovative catalyst design strategies—including alloying, heterostructuring, and morphological control—aimed at enhancing activity, selectivity, and stability for the production of value-added C_1-C_3 products. Through detailed structure–activity correlations, we underscored the pivotal role of site-specific active center engineering in steering product distribution toward desired compounds such as DHA, GLA, and FA.

Despite significant progress, critical challenges impede the practical implementation of GEOR. These include intrinsically sluggish reaction kinetics, insufficient long-term catalyst stability, limited product selectivity due to parallel reaction pathways, and scalability issues inherent to conventional electrolyzer configurations. Moreover, while numerous studies have focused on empirical catalyst optimization, fundamental mechanistic studies and integrated electrolysis system designs remain underexplored. To address these challenges, the following research priorities are proposed:

(i) Advanced multimetallic catalyst design: Future efforts should prioritize non-noble metal-based and high-entropy systems to reduce costs while maintaining high performance, especially the production of C_3 products. high-entropy alloy sites and high-entropy oxides/ phosphides endows the catalytic interface with distinctive physicochemical properties. Furthermore, these high-entropy carriers can synergize with single-atom active sites to modulate catalytic behavior, thereby optimizing reaction kinetics and selectivity. Rational construction of low-dimensional architectures (e.g., 1D nanowires, 2D nanosheets, and porous frameworks) can enhance mass transport, expose abundant active sites, and improve electrochemical stability. Special attention should be paid to optimizing synergistic interactions between multiple metals and stabilizing active species under operational conditions.

(ii) Integrated reaction systems: The coupling of GEOR with value-added cathodic reactions—such as nitrate reduction to ammonia, CO_2 electroreduction, or hydrogenation of organic compounds—presents a promising route to improve overall process economics and energy efficiency. Furthermore, the in situ conversion of GEOR-derived C_1–C_3 products into higher-value derivatives should be explored. Additionally, the development of acidic or solid-state electrolyte systems could facilitate the production of acid-sensitive oxidation products and mitigate carbonate formation issues associated with alkaline media.

(iii) Artificial intelligence and machine learning enable high-throughput screening of a vast library of catalytic materials, thereby drastically shorten-

ing the material design cycle. This advantage is particularly pronounced for complex systems such as high-entropy materials. Moreover, to steer glycerol electrochemical oxidation toward distinct value-added products, tailored synthetic strategies and deliberate heteroatom doping are imperative for engineering an electronically favorable microenvironment at the catalyst surface, which kinetically prioritizes the formation of target products by modulating the adsorption energy of reaction intermediates and the activation barrier of rate-determining steps.

(iv) Mechanistic and operational insights: Advanced in situ/operando characterization techniques for transient intermediates—including in situ TEM, Raman, FTIR, and synchrotron-based X-ray spectroscopy—are essential to decipher the dynamic evolution of active sites and reaction intermediates under working conditions. Complementary theoretical studies and microkinetic modeling will help establish definitive reaction mechanisms. Furthermore, engineering the electrode–electrolyte interface to promote glycerol adsorption and product desorption—for instance, by creating hydrophilic and aerophobic local environments—can significantly enhance reaction rates and suppress over-oxidation.

(v) Faradaic efficiency is a critical metric for evaluating the charge utilization efficiency of electrocatalysts toward target products in electrochemical reactions (see Table 1). Complementarily, turnover frequency (TOF) is an indispensable parameter for evaluating intrinsic catalytic activity, as it normalizes reaction rates to the number of active sites. Notably, TOF has been rarely reported in glycerol electrooxidation reaction (GEOR) studies to date. Given its significance, researchers should analyze TOF for future GEOR catalyst development. Notably, Faradaic efficiency and TOF are strongly dependent on reaction conditions, including applied potentials, temperatures, and reactant concentrations, which must be rigorously considered during data interpretation.

(vi) GEOR is predominantly conducted in alkaline electrolytes, which facilitate rapid reaction kinetics. However, this operational choice induces the conversion of products into salt forms (e.g., carboxylates), thereby increasing downstream separation costs. In contrast, acidic electrolytes preserve the native molecular structure of target products (e.g., free carboxylic acids) but present inherent challenges, including sluggish anodic reaction kinetics, dissolution of active metal sites, and carbon support corrosion. Leveraging the cost advantage of non-precious metallic species, future research should prioritize rational structural engineering (like single-atom catalysts and metal nitrides) to endow non-precious metallic catalysts with high selectivity and high activity for the synthesis of high-value C_2/C_3 products under low applied potential and acidic conditions.

Looking forward, achieving techno-economic viability will require the integration of flow reactors, advanced product separation units, and scalable electrocatalyst manufacturing processes. Interdisciplinary efforts combining catalyst design, reactor engineering, and process optimization will be crucial to advance GEOR from laboratory curiosity toward sustainable and economically feasible electrochemical manufacturing.

REFERENCES

1. Husna M., Tabak Y. and Yıldız M. (2024). Glycerol as a feedstock for chemical synthesis. *ChemBioEng Rev.* **11**:e202400010. DOI:10.1002/cben.202400010
2. Sun H., Yang M., Gao Z., et al. (2023). Economic and environmental evaluation for a closed loop of crude glycerol bioconversion to biodiesel. *J. Biotechnol.* **366**:65–71. DOI:10.1016/j.jbiotec.2023.03.001
3. Zhang S., Guan W., Sun H., et al. (2023). Intermittent energization improves microbial electrolysis cell-assisted thermophilic anaerobic co-digestion of food waste and spent mushroom substance. *Bioresour. Technol.* **370**:128577. DOI:10.1016/j.biortech.2023.128577
4. Kazimierowicz J., Dębowski M., Zieliński M., et al. (2024). The biosynthesis of liquid fuels and other value-added products based on waste glycerol—a comprehensive review and bibliometric analysis. *Energies* **17**:3035. DOI:10.3390/en17123035
5. Fasanya O. O., Osigbesan A. A. and Avbenake O. P. (2021). Biodiesel production from non-edible and waste lipid sources. *Biodiesel Technol. Appl.* **15**:389–427. DOI:10.1002/9781119724957.ch15
6. Ray A., Kundu P. and Ghosh A. (2023). Reconstruction of a genome-scale metabolic model of scenedesmus obliquus and its application for lipid production under three trophic modes. *ACS Synth. Biol.* **12**:3463–3481. DOI:10.1021/acssynbio.3c00516
7. Murphy D. J., Goggin K. and Paterson R. R. M. (2021). Oil palm in the 2020s and beyond: challenges and solutions. *CABI Agric. Biosci.* **2**:39. DOI:10.1186/s43170-021-00058-3
8. Lazar Z., Liu N. and Stephanopoulos G. (2018). Holistic approaches in lipid production by yarrowia lipolytica. *Trends Biotechnol.* **36**:1157–1170. DOI:10.1016/j.tibtech.2018.06.007
9. Hill J., Nelson E., Tilman D., et al. (2006). Environmental, economic, and energetic costs and benefits of biodiesel and ethanol biofuels. *Proc. Natl. Acad. Sci. U.S.A.* **30**:11206–11210. DOI:10.1073/pnas.0604600103
10. Beopoulos A., Nicaud J-M. and Gaillardin C. (2011). An overview of lipid metabolism in yeasts and its impact on biotechnological processes. *Appl. Microbiol. Biotechnol.* **4**:1193–1206. DOI:10.1007/s00253-011-3212-8
11. Becerra-Ruiz J. D., Gonzalez-Huerta R. G., Gracida J., et al. (2019). Using green-hydrogen and bioethanol fuels in internal combustion engines to reduce emissions. *Int. J. Hydrogen Energy* **44**:12324–12332. DOI:10.1016/j.ijhydene.2019.02.211
12. Xu X., Sharma P., Shu S., et al. (2021). Global greenhouse gas emissions from animal-based foods are twice those of plant-based foods. *Nat. Food* **2**:724–732. DOI:10.1038/s43016-021-00358-x
13. Bowling R. A. and Larrabee G. B. (1983). Surface characterization. *Anal. Chem.* **55**:133–156. DOI:10.1021/a19900159
14. Eryilmaz T., Yesilyurt M. K., Cesur C., et al. (2016). Biodiesel production potential from oil seeds in Turkey. *Renew. Sust. Energ. Rev.* **58**:842–851. DOI:10.1016/j.rser.2015.12.172
15. Naylor R. L. and Higgins M. M. (2018). The rise in global biodiesel production: implications for food security. *Global Food Secur.* **16**:75–84. DOI:10.1016/j.gfs.2017.10.004
16. Wang H., Li H., Lee C. K., et al. (2024). A systematic review on utilization of biodiesel-derived crude glycerol in sustainable polymers preparation. *Int. J. Biol. Macromol.* **261**:129536. DOI:10.1016/j.ijbiomac.2024.129536
17. Abusweireh R. S., Rajamohan N. and Vasseghian Y. (2022). Enhanced production of biodiesel using nanomaterials: a detailed review on the mechanism and influencing factors. *Fuel* **319**:123862. DOI:10.1016/j.fuel.2022.123862
18. Zhao J., Hao S., Zhao P., et al. (2025). On-demand catalytic platform for glycerol upgrade and utilization. *J. Am. Chem. Soc.* **147**:9210–9219. DOI:10.1021/jacs.4c13603
19. Jindapon W., Ruengyoo S., Kuchonthara P., et al. (2020). Continuous production of fatty acid methyl esters and high-purity glycerol over a dolomite-derived extrudate catalyst in a countercurrent-flow trickle-bed reactor. *Renew. Energy* **157**:626–636. DOI:10.1016/j.renene.2020.05.066
20. Çakmak A. and Özcan H. (2020). Biofuel additive production from glycerol and determination of its effect on some fuel properties. *SN Appl. Sci.* **2**:1–10. DOI:10.1007/s42452-020-03308-7
21. Moklis M. H., Cheng S. and Cross J. S. (2023). Current and future trends for crude glycerol upgrading to high value-added products. *Sustainability* **15**:2979. DOI:10.3390/su15042979
22. Zhang J., Yang J., Zhang H., et al. (2021). Research status and future development of biomass liquid fuels. *BioResources* **16**:4523–4543. DOI:10.15376/biores.16.2.Zhang
23. Almeida E. L., Olivo J. E. and Andrade C. M. G. (2023). Production of biofuels from glycerol from the biodiesel production process—a brief review. *Fermentation* **9**:869. DOI:10.3390/fermentation9100869
24. Anto L., Warykas S. W., Torres-Gonzalez M., et al. (2020). Milk polar lipids: underappreciated lipids with emerging health benefits. *Nutrients* **12**:1001. DOI:10.3390/nu12041001
25. Kalus K., Konkol D., Korczyński M., et al. (2020). Effect of biochar diet supplementation on chicken broilers performance, NH_3 and odor emissions and meat consumer acceptance. *Animals* **10**:1539. DOI:10.3390/ani10091539
26. Ezequiel J. M. B., Sancanari J. B. D., Machado Neto O. R., et al. (2015). Effects of high concentrations of dietary crude glycerin on dairy cow productivity and milk quality. *J. Dairy Sci.* **98**:8009–8017. DOI:10.3168/jds.2015-9448
27. Lomander H., Frössling J., Ingvartsen K. L., et al. (2012). Supplemental feeding with glycerol or propylene glycol of dairy cows in early lactation—effects on metabolic status, body condition, and milk yield. *J. Dairy Sci.* **95**:2397–2408. DOI:10.3168/jds.2011-4535
28. Kim H. J., Kim Y., Lee D., et al. (2017). Coproducing value-added chemicals and hydrogen with electrocatalytic glycerol oxidation technology: experimental and techno-economic investigations. *ACS Sustainable Chem. Eng.* **5** 6626-6634. DOI:10.1021/acssuschemeng.7b00868.
29. Worz N., Brandner A. and Claus P. (2010). Platinum–bismuth-catalyzed oxidation of glycerol: kinetics and the origin of selective deactivation. *J. Phys. Chem. C* **114**:1164–1172. DOI:10.1021/jp909412h
30. Xiong L., Yu Z., Cao H., et al. (2021). Converting glycerol into valuable trioses by $Cu^{δ+}$-single-atom-decorated WO_3 under visible light. *Angew. Chem. Int. Ed.* **63**:e202318461. DOI:10.1002/anie.202318461
31. Yang T. and Shen Y. (2023). coupling glycerol conversion with hydrogen production using alloyed electrocatalysts. *Langmuir* **39**:12855–12864. DOI:10.1021/acs.langmuir.3c01751
32. An Z., Zhang Z., Huang Z., et al. (2022). Pt(1) enhanced C-H activation synergistic with Pt(n) catalysis for glycerol cascade oxidation to glyceric acid. *Nat. Commun.* **13**:5467. DOI:10.1038/s41467-022-33038-w

33. Kim H. J., Lee J., Green S. K., et al. (2014). Selective glycerol oxidation by electrocatalytic dehydrogenation. *ChemSusChem* **7**:1051–1056. DOI:10.1002/cssc.201301218
34. Wang S., Lin Y., Li Y., et al. (2025). Nanoscale high-entropy surface engineering promotes selective glycerol electro-oxidation to glycerate at high current density. *Nat. Nanotechnol.* **20**:646–655. DOI:10.1038/s41565-025-01881-9
35. Nunotani N., Morita K. and Imanaka N. (2025). Efficient production of hydroxypyruvic acid from glycerol using Pt/$ZrSn_{1-x}Bi_xO_{4-\delta}$/SBA-16 catalysts. *ACS Sustainable Chem. Eng.* **13**:8206–8211. DOI:10.1021/acssuschemeng.5c03264
36. Teng Z., Zhang Z., Tu Y., et al. (2025). Asymmetric photooxidation of glycerol to hydroxypyruvic acid over Rb–Ir catalytic pairs on poly(heptazine imides). *Nat. Nanotechnol.* **20**:815–824. DOI:10.1038/s41565-025-01897-1
37. Zhang Z., Xin L. and Li W. (2012). Electrocatalytic oxidation of glycerol on Pt/C in anion-exchange membrane fuel cell: cogeneration of electricity and valuable chemicals. *Appl. Catal. B Environ.* **119-120**:40-48. DOI:10.1016/j.apcatb.2012.02.009.
38. Behr A., Eilting J., Irawadi K., et al. (2008). Improved utilisation of renewable resources: new important derivatives of glycerol. *Green Chem.* **10**:13–30. DOI:10.1039/B710561D
39. Fang Z., Ding Y., Su Z., et al. (2025). Highly selective electrooxidation of glycerol to tartronic acid over a single-atom rhodium catalyst supported on indium oxide. *Small* **21**:2500123. DOI:10.1002/smll.202500123
40. Ciriminna R. and Pagliaro M. (2003). One-pot homogeneous and heterogeneous oxidation of glycerol to ketomalonic acid mediated by TEMPO. *Adv. Synth. Catal.* **345**:383–388. DOI:10.1002/adsc.200390043
41. Wang J., Liu Y., Wang J., et al. (2023). Cooperative catalysis of carbon supported zinc salts hybrid for efficient conversion of fructose to ethyl lactate. *Chem. Eng. J.* **468**:143670. DOI:10.1016/j.cej.2023.143670
42. Kang N. K., Kim M., Baek K., et al. (2022). Photoautotrophic organic acid production: glycolic acid production by microalgal cultivation. *Chem. Eng. J.* **433**:133636. DOI:10.1016/j.cej.2021.133636
43. Oh L. S., Park M., Park Y. S., et al. (2023). How to change the reaction chemistry on nonprecious metal oxide nanostructure materials for electrocatalytic oxidation of biomass-derived glycerol to renewable chemicals. *Adv. Mater.* **35**:2203285. DOI:10.1002/adma.202203285
44. Morales D. M., Jambrec D., Kazakova M. A., et al. (2022). Electrocatalytic conversion of glycerol to oxalate on Ni oxide nanoparticles-modified oxidized multiwalled carbon nanotubes. *ACS Catal.* **12**:982–992. DOI:10.1021/acscatal.1c04150
45. Zhang Z. and Huber G. W. (2018). Catalytic oxidation of carbohydrates into organic acids and furan chemicals. *Chem. Soc. Rev.* **47**:1351–1390. DOI:10.1039/C7CS00213K
46. Le T. H., Zuo Y., Chatti M., et al. (2025). Coupling of CuO@$NiBiO_x$ catalyzed glycerol oxidation to carbon dioxide reduction reaction for enhanced energy efficiency. *Angew. Chem. Int. Ed.* **64**:e202502617. DOI:10.1002/anie.202502617
47. Verma S., Lu S. and Kenis P. J. A. (2019). Co-electrolysis of CO_2 and glycerol as a pathway to carbon chemicals with improved technoeconomics due to low electricity consumption. *Nat. Energy* **4**:466–474. DOI:10.1038/s41560-019-0374-6
48. Zhou Y., Shen Y. and Xi J. (2019). Seed-mediated synthesis of Pt_xAu_y@Ag electrocatalysts for the selective oxidation of glycerol. *Appl. Catal. B Environ.* **245**:604–612. DOI:10.1016/j.apcatb.2019.01.009
49. Hone C. A. and Kappe C. O. (2018). The use of molecular oxygen for liquid phase aerobic oxidations in continuous flow. *Top. Curr. Chem.* **377**:2. DOI:10.1007/s41061-018-0226-z
50. James O. O., Sauter W. and Schröder U. (2018). Towards selective electrochemical conversion of glycerol to 1,3-propanediol. *RSC Adv.* **8**:10818–10827. DOI:10.1039/C8RA00711J
51. Moklis M. H., Avian C., Shuo C., et al. (2025). GAN-driven discovery of low-cost non-noble metallic electrocatalysts for glycerol electroreduction. *Electrochim. Acta* **539**:147096. DOI:10.1016/j.electacta.2025.147096
52. Moklis M. H., Shuo C., Boonyubol S., et al. (2024). Electrochemical valorization of glycerol via electrocatalytic reduction into biofuels: a review. *ChemSusChem* **17**:e202300990. DOI:10.1002/cssc.202300990
53. Wu D., Liu S., Nie Y., et al. (2025). Electrocatalytic upgrading of glycerol into high-value products: Catalyst design, process engineering, and economic assessment. *Chem. Eng. J.* **518**:164511. DOI:10.1016/j.cej.2025.164511
54. Li Y., Wei X., Pan R., et al. (2024). PtAu alloying-modulated hydroxyl and substrate adsorption for glycerol electrooxidation to C3 products. *Energy Environ. Sci.* **17**:4205–4215. DOI:10.1039/D4EE00485J
55. Ma L., Miao Y., Yang J., et al. (2024). Promoting electrocatalytic glycerol C-C bond cleavage to FA coupled with H_2 production over a $Cu_xNi_{2-x}P$ catalyst. *Adv. Energy Mater.* **14**:2401061. DOI:10.1002/aenm.202401061
56. Neyts E. C., Ostrikov K. K., Sunkara M. K., et al. (2015). Plasma catalysis: synergistic effects at the nanoscale. *Chem. Rev.* **115**:13408–46. DOI:10.1021/acs.chemrev.5b00362
57. Deng Y. J., Tian N., Zhou Z. Y., et al. (2012). Alloy tetrahexahedral Pd–Pt catalysts: enhancing significantly the catalytic activity by synergy effect of high-index facets and electronic structure. *Chem. Sci.* **3**:1157–1161. DOI:10.1039/C2SC00723A
58. Jiang K., Zhao D., Guo S., et al. (2017). Efficient oxygen reduction catalysis by subnanometer Pt alloy nanowires. *Sci. Adv.* **3**:e1601705. DOI:10.1126/sciadv.1601705
59. Xia Z., Ma C., Fan Y., et al. (2024). Vacancy optimized coordination on nickel oxide for selective electrocatalytic oxidation of glycerol. *ACS Catal.* **14**:1930–1938. DOI:10.1021/acscatal.3c04568
60. Chen W., Shi J., Wu Y., et al. (2024). Vacancy-induced catalytic mechanism for alcohol electrooxidation on nickel-based electrocatalyst. *Angew. Chem. Int. Ed.* **63**:e202316449. DOI:10.1002/anie.202316449
61. Tran G. S., Chen C. J., Maeda S., et al. (2024). Tuning selectivity toward three-carbon product of glycerol electrooxidation in borate buffer through manipulating borate/glycerol molar ratio. *J. Catal.* **438**:115715. DOI:10.1016/j.jcat.2024.115715
62. Chen P. and Huang S. (2022). Quaternary PdCuNiP porous nanosheets with enhanced electrochemical performance in the ethanol oxidation reaction. *Inorg. Chem.* **61**:14470–14476. DOI:10.1021/acs.inorgchem.2c02597
63. Minichová M., Priamushko T., Hutzler A., et al. (2024). Electrochemical dissolution of PtRu/C: Effect of potential, fuels, and temperature. *Electrochim. Acta* **502**:144764. DOI:10.1016/j.electacta.2024.144764
64. Brix A. C., Morales D. M., Braun M., et al. (2021). Electrocatalytic oxidation of glycerol using solid - state synthesised nickel boride: impact of key electrolysis parameters on product selectivity. *ChemElectroChem* **8**:2336–2342. DOI:10.1002/celc.202100739
65. Barman K., Askarova G., Jia R., et al. (2023). Efficient voltage-driven oxidation of water and alcohols by an organic molecular catalyst directly attached to a carbon electrode. *J. Am. Chem. Soc.* **145**:5786–5794. DOI:10.1021/jacs.2c12775
66. Angelucci C. A., Varela H., Tremiliosi-Filho G., et al. (2013). The significance of non-covalent interactions on the electro-oxidation of alcohols on Pt and Au in alkaline media. *Electrochem. Commun.* **33**:10–13. DOI:10.1016/j.elecom.2013.03.039
67. Yukuhiro V. Y., Vicente R. A., Fernandez P. S., et al. (2024). Alkaline-metal cations affect Pt deactivation for the electrooxidation of small organic molecules by affecting the formation of inactive Pt oxide. *J. Am. Chem. Soc.* **146**:27745–27754. DOI:10.1021/jacs.4c09590
68. Huang X., Zou Y. and Jiang J. (2021). Electrochemical oxidation of glycerol to dihydroxyacetone in borate buffer: enhancing activity and selectivity by borate–polyol coordination chemistry. *ACS Sustainable Chem. Eng.* **9**:14470–14479. DOI:10.1021/acssuschemeng.1c04795
69. Chen W., Zhang L., Xu L., et al. (2024). Pulse potential mediated selectivity for the electrocatalytic oxidation of glycerol to glyceric acid. *Nat. Commun.* **15**:2420. DOI:10.1038/s41467-024-46752-4
70. Xia T., Yang J., Ren Q., et al. (2025). Promoting alcohols electrooxidation coupled with hydrogen production via asymmetric pulse potential strategy. *Angew. Chem. Int. Ed.* **64**:e202420992. DOI:10.1002/anie.202420992
71. Guschakowski M. and Schröder U. (2021). Direct and indirect electrooxidation of glycerol to value-added products. *ChemSusChem* **14**:5216–5225. DOI:10.1002/cssc.202100556
72. Kornienko G. V., Chaenko N. V. and Kornienko V. L. (2015). Indirect electrocatalytic oxidation of glycerin on platinum electrode in acidic electrolyte involving active oxygen forms. *Russ. J. Electrochem.* **51**:1115-1118. DOI 10.1134/S1023193515110063.
73. Tang H. T., Jia J. S. and Pan Y. M. (2020). Halogen-mediated electrochemical organic synthesis. *Org. Biomol. Chem.* **18**:5315–5333. DOI:doi.org/10.1039/D0OB01008A. DOI:10.1039/D0OB01008A
74. Lian F., Xu K. and Zeng C. (2021). Indirect electrosynthesis with halogen ions as mediators. *Chem. Rec.* **21**:2290–2305. DOI:10.1002/tcr.202100036
75. Liu Y. J., Hu C. Y. and Lo S. L. (2019). Direct and indirect electrochemical oxidation of amine-containing pharmaceuticals using graphite electrodes. *J. Hazard. Mater.* **366**:592–605. DOI:10.1016/j.jhazmat.2018.12.037
76. Wang F. and Stahl S. S. (2020). Electrochemical oxidation of organic molecules at lower overpotential: accessing broader functional group compatibility with electron–proton transfer mediators. *Acc. Chem. Res.* **53**:561–574. DOI:10.1021/acs.accounts.9b00544
77. Houache M. S. E., Hughes K., Ahmed A., et al. (2019). Electrochemical valorization of glycerol on Ni-rich bimetallic NiPd nanoparticles: insight into product selectivity using in situ polarization modulation infrared-reflection absorption spectroscopy. *ACS Sustainable Chem. Eng.* **7**:14425–14434. DOI:10.1021/acssuschemeng.9b01070
78. He Z., Hwang J., Gong Z., et al. (2022). Promoting biomass electrooxidation via modulating proton and oxygen anion deintercalation in hydroxide. *Nat. Commun.* **13**:3777. DOI:10.1038/s41467-022-31484-0
79. Valter M., dos Santos E. C., Pettersson L. G. M., et al. (2021). Selectivity of the first two glycerol dehydrogenation steps determined using scaling relationships. *ACS Catal.* **11**:3487–3497. DOI:10.1021/acscatal.0c04186
80. Valter M., dos Santos E. C., Pettersson L. G. M., et al. (2020). Partial electrooxidation of glycerol on close-packed transition metal surfaces: insights from first-principles calculations. *J. Phys. Chem. C* **124**:17907–17915. DOI:10.1021/acs.jpcc.0c04002
81. Kwon Y., Schouten K. J. P. and Koper M. T. M. (2011). Mechanism of the catalytic oxidation of glycerol on polycrystalline gold and platinum electrodes. *ChemCatChem* **3**:1176–1185. DOI:10.1002/cctc.201100023
82. Mendes P. C. D., Costa-Amaral R., Gomes J. F., et al. (2019). The influence of

hydroxy groups on the adsorption of three-carbon alcohols on Ni(111), Pd(111) and Pt(111) surfaces: a density functional theory study within the D3 dispersion correction. *Phys. Chem. Chem. Phys.* **21**:8434–8444. DOI:10.1039/c9cp00752k
83. Amaral R. C., Tereshchuk P., Seminovski Y., et al. (2017). The role of low-coordinated sites on the adsorption of glycerol on defected Ptn/Pt(111) substrates: a density functional investigation within the D3 van der Waals correction. *J. Phys. Chem. C* **121**:3445–3454. DOI:10.1021/acs.jpcc.6b12238
84. Luo H., Yukuhiro V. Y., Fernández P. S., et al. (2022). Role of Ni in PtNi bimetallic electrocatalysts for hydrogen and value-added chemicals coproduction via glycerol electrooxidation. *ACS Catal.* **12**:14492–14506. DOI:10.1021/acscatal.2c03907
85. Ghosh S., Bagchi D., Mondal I., et al. (2024). Deciphering the role of nickel in electrochemical organic oxidation reactions. *Adv. Energy Mater.* **14**:2400696. DOI:10.1002/aenm.202400696
86. Houache M. S. E., Cossar E., Ntais S., et al. (2018). Electrochemical modification of nickel surfaces for efficient glycerol electrooxidation. *J. Power Sources* **375**:310–319. DOI:10.1016/j.jpowsour.2017.08.089
87. Serov A., Asset T., Padilla M., et al. (2016). Highly-active Pd–Cu electrocatalysts for oxidation of ubiquitous oxygenated fuels. *Appl. Catal. B Environ.* **191**:76–85. DOI:10.1016/j.apcatb.2016.03.016
88. Du J., Qin Y., Dou T., et al. (2022). Copper nanoparticles dotted on copper sulfide nanosheets for selective electrocatalytic oxidation of glycerol to FA. *ACS Appl. Nano Mater.* **5**:10174–10182. DOI:10.1021/acsanm.2c00323
89. Fan R. Y., Zhai X. J., Qiao W. Z., et al. (2023). Optimized electronic modification of S-doped CuO induced by oxidative reconstruction for coupling glycerol electrooxidation with hydrogen evolution. *Nano-micro Lett.* **15**:190. DOI:10.1007/s40820-023-01159-6
90. Sapner V. S., Tanwade P. D., Munde A. V., et al. (2023). Cobalt/cobalt oxide nanorods-decorated Reduced graphene oxide (Co/Co_3O_4-rGO) for enhanced electrooxidation of glycerol. *ACS Appl. Nano Mater.* **6**:16414–16423. DOI:10.1021/acsanm.3c02636
91. Xi N., Zang Y., Sun X., et al. (2023). Polyhedral coordination determined Co - O activity for electrochemical oxidation of biomass alcohols. *Adv. Energy Mater.* **13**:2301572. DOI:10.1002/aenm.202301572
92. Goetz M. K., Usman E. and Choi K. S. (2023). Understanding and suppressing C–C cleavage during glycerol oxidation for C3 chemical production. *ACS Catal.* **13**:15758–15769. DOI:10.1021/acscatal.3c03365
93. González-Cobos J., Baranton S. and Coutanceau C. (2016). A systematic in situ infrared study of the electrooxidation of C3 alcohols on carbon-supported Pt and Pt–Bi catalysts. *J. Phys. Chem. C* **120**:7155–7164. DOI:10.1021/acscatal.3c03365
94. Li Y., Wei X., Han S., et al. (2021). MnO_2 electrocatalysts coordinating alcohol oxidation for ultra-durable hydrogen and chemical productions in acidic solutions. *Angew. Chem. Int. Ed.* **60**:21464–21472. DOI:10.1002/anie.202107510
95. Mao Z., Jia L., Mao X., et al. (2024). Bismuth single-atom alloying of palladium nanosheets promotes selective electrochemical valorization of glycerol to C3 products. *J. Mater. Chem. A* **12**:24136–24143. DOI:10.1039/D4TA03892D
96. Yang H., Vijaykumar G., Chen Z., et al. (2023). In situ reconstruction of helical iron borophosphate precatalyst toward durable industrial alkaline water electrolysis and selective oxidation of alcohols. *Adv. Funct. Mater.* **33**:2303702. DOI:10.1002/adfm.202303702
97. Sun T., Chen J., Lao X., et al. (2022). Unveiling the synergistic effects of monodisperse sea urchin-like PdPb alloy nanodendrites as stable electrocatalysts for ethylene glycol and glycerol oxidation reactions. *Inorg. Chem.* **61**:10220–10227. DOI:10.1021/acs.inorgchem.2c01566
98. Lari G. M., Mondelli C. and Pérez-Ramírez J. (2015). Gas-phase oxidation of glycerol to dihydroxyacetone over tailored iron zeolites. *ACS Catal.* **5**:1453–1461. DOI:10.1021/cs5019056
99. Pagliaro M., Ciriminna R., Kimura H., et al. (2007). From glycerol to value - added products. *Angew. Chem. Int. Ed.* **46**:4434–4440. DOI:10.1002/anie.200604694
100. Painter R. M., Pearson D. M. and Waymouth R. M. (2010). Selective catalytic oxidation of glycerol to dihydroxyacetone. *Angew. Chem. Int. Ed.* **49**:9456–9459. DOI:10.1002/anie.201004063
101. Huang N., Zhang Z., Lu Y., et al. (2021). Assembly of platinum nanoparticles and single-atom bismuth for selective oxidation of glycerol. *J. Mater. Chem. A* **9**:25576–25584. DOI:10.1039/D1TA07262E
102. Kunitski M., Eicke N., Huber P., et al. (2019). Double-slit photoelectron interference in strong-field ionization of the neon dimer. *Nat. Commun.* **10**:1. DOI:10.1038/s41467-018-07882-8
103. Zhao S., Dai Z., Guo W., et al. (2019). Highly selective oxidation of glycerol over $Bi/Bi_{3.64}Mo_{0.36}O_{6.55}$ heterostructure: dual reaction pathways induced by photogenerated $^1O_2$ and holes. *Appl. Catal. B Environ.* **244**:206-214. DOI:10.1016/j.apcatb.2018.11.047.
104. Hiroshi K., Keiichi T., Tatsushi W., et al. (1993). Selective oxidation of glycerol on a platinum-bismuth catalyst. *Appl. Catal. A Gen.* **96**:217–228. DOI:10.1016/0926-860X(90)80011-3
105. Liu C., Hirohara M., Maekawa T., et al. (2020). Selective electro-oxidation of glycerol to dihydroxyacetone by a non-precious electrocatalyst–CuO. *Appl. Catal. B Environ.* **265**:118543. DOI:10.1016/j.apcatb.2019.118543
106. Huang Z., Ren H., Guo J., et al. (2024). High DHA selectivity and low-cost electrode for glycerol oxidation: CuO regulates MnO_2 electron density to promote DHA desorption. *Appl. Catal. B Environ.* **351**:123986. DOI:10.1016/j.apcatb.2024.123986
107. Braun M., Santana C. S., Garcia A. C., et al. (2023). From waste to value–Glycerol electrooxidation for energy conversion and chemical production. *Curr. Opin. Green Sustainable Chem.* **41**:100829. DOI:10.1016/j.cogsc.2023.100829
108. Lee D., Kim Y., Han H., et al. (2020). Atomic-layer-deposited SnO_2 on Pt/C prevents sintering of Pt nanoparticles and affects the reaction chemistry for the electrocatalytic glycerol oxidation reaction. *J. Mater. Chem. A* **8**:15992–16005. DOI:10.1039/D0TA02509G
109. Chen W., Zhang L., Xu L., et al. (2024). Pulse potential mediated selectivity for the electrocatalytic oxidation of glycerol to glyceric acid. *Nat. Commun.* **15**:2420. DOI:10.1038/s41467-024-46752-4
110. Cychy S., Lechler S. and Muhler M. (2021). Selective anodic oxidation of solketal as acetal - protected glycerol over nickel boride in alkaline media to glyceric acid. *ChemElectroChem* **9**:e202101214. DOI:10.1002/celc.202101214
111. Kumari B., Braun M., Cychy S., et al. (2023). Electrooxidation of the glycerol derivative solketal over Cu–Co hydroxycarbonates to enable the synthesis of glyceric acid. *ChemElectroChem* **10**:e202300018. DOI:10.1002/celc.202300018
112. Zhang J., Kumari B., Quast T., et al. (2024). Surface reconstruction induced by preconditioning in different electrolytes impacts electrooxidation of solketal on multi - metal - based catalysts. *Adv. Funct. Mater.* **35**:2419911. DOI:10.1002/adfm.202419911
113. Yang J., Xia T., Li H., et al. (2024). Evaluation of active oxygen species derived from water splitting for electrocatalytic organic oxidation. *Angew. Chem. Int. Ed.* **64**:e202413457. DOI:10.1002/anie.202413457
114. Costa Santos J. B., Vieira C., Crisafulli R., et al. (2020). Promotional effect of auxiliary metals Bi on Pt, Pd, and Ag on Au, for glycerol electrolysis. *Int. J. Hydrog. Energy* **45**:25658–25671. DOI:10.1016/j.ijhydene.2019.11.225
115. Pagliaro M. V., Bruni F., Oberhauser W., et al. (2025). Hydrogen and high-value-added chemicals from glycerol electroreforming using a highly efficient and selective ligand-stabilized PdCu catalyst. *ACS Sustainable Chemi. Eng.* **13**:4975–4987. DOI:10.1021/acssuschemeng.4c09284
116. Terekhina I. and Johnsson M. (2024). Improving glycerol electrooxidation performance on nanocubic PtCo Catalysts. *ACS Appl. Mater. Interfaces* **16**:56987–56996. DOI:10.1021/acsami.4c10219
117. Huang B., Yan J., Li Z., et al. (2024). Anode-electrolyte interfacial acidity regulation enhances electrocatalytic performances of alcohol oxidations. *Angew. Chem. Int. Ed.* **63**:e202409419. DOI:10.1002/anie.202409419
118. Naik K. M., Hashisake K., Hamada T., et al. (2022). Intermetallic PdZn nanoparticles loaded on deficient TiO_2 nanosheets as a support: a bifunctional electrocatalyst for oxygen reduction in PEMFCs and the glycerol oxidation reactions. *J. Mater. Chem. A* **10**:13987–13997. DOI:10.1039/d2ta03736j
119. Benipal N., Qi J., Liu Q., et al. (2017). Carbon nanotube supported PdAg nanoparticles for electrocatalytic oxidation of glycerol in anion exchange membrane fuel cells. *Appl. Catal. B Environ.* **210**:121–130. DOI:10.1016/j.apcatb.2017.02.082
120. Wang C. Y., Yu Z. Y., Li G., et al. (2020). Intermetallic PtBi nanoplates with high catalytic activity towards electro-oxidation of formic acid and glycerol. *ChemElectroChem.* **7**:239–245. DOI:10.1002/celc.201901818
121. Holade Y., Servat K., Napporn T. W., et al. (2015). Electrocatalytic properties of nanomaterials synthesized from "Bromide Anion Exchange" method-investigations of glucose and glycerol oxidation. *Electrochim. Acta* **162**:205–214. DOI:10.1016/j.electacta.2014.11.072
122. Cassani A., Tuleushova N., Wang Q., et al. (2021). Fe-modified Pd as an effective multifunctional electrocatalyst for catalytic oxygen reduction and glycerol oxidation reactions in alkaline media. *ACS Appl. Energy Mater.* **4**:9944–9960. DOI:10.1021/acsaem.1c01920
123. Brix A. C., Dreyer M., Koul A., et al. (2022). Structure - performance relationship of $LaFe_{1-x}Co_xO_3$ electrocatalysts for oxygen evolution, isopropanol oxidation, and glycerol oxidation. *ChemElectroChem* **9**:e202200092. DOI:10.1002/celc.202200092
124. Houache M. S. E., Safari R., Nwabara U. O., et al. (2020). Selective electrooxidation of glycerol to formic acid over carbon supported $Ni_{1-x}M_x$ (M = Bi, Pd, and Au) nanocatalysts and coelectrolysis of CO_2. *ACS Appl. Energy Mater.* **3**:8725–8738. DOI:10.1021/acsaem.0c01282
125. Wang Y., Ge R., Liu X., et al. (2024). An anion leaching strategy towards metal oxyhydroxides synthesis for electrocatalytic oxidation of glycerol. *Acta Phys. Chim. Sin.* **40**:2307019. DOI:10.3866/PKU.WHXB202307019
126. Zheng Y., Kang Z., Li H., et al. (2025). Hierarchically structured $CuNiP/CuO_x$-VP nanoarrays construction by heteroatom doping boosting glycerol valorization at industrial-level current density. *Adv. Funct. Mater.* **35**:2412810. DOI:10.1002/adfm.202412810
127. Chen H., Gao R. T., Su K., et al. (2025). Re and Ru co-doped transition metal alloy as a bifunctional catalyst for electrooxidation of glycerol to FA coupled with H_2 production. *Angew. Chem. Int. Ed.* **64**:e202501766. DOI:10.1002/anie.202501766
128. Wu Y., Fang W., Li M., et al. (2024). Implanting CuNi alloy into $NiVO_x$ for H_2 evolution with ultralow overpotential and highly selective FA production. *ACS Sustainable Chem. Eng.* **12**:9207–9221. DOI:10.1021/acssuschemeng.4c01950
129. Chen Z., Liu C., Zhao X., et al. (2019). Promoted glycerol oxidation reaction in an interface-confined hierarchically structured catalyst. *Adv. Mater.* **31**:e1804763. DOI:10.1002/adma.201804763

130. Zhu Y., Qian Q., Chen Y., et al. (2023). Biphasic transition metal nitride electrode promotes nucleophile oxidation reaction for practicable hybrid water electrocatalysis. *Adv. Funct. Mater.* **33**:2300547. DOI:10.1002/adfm.202300547
131. Ma J., Tian Y., Li J., et al. (2024). Construction of Ni_3S_2/NiFe LDH heterostructure as bifunctional catalyst for energy-saving hydrogen evolution and co-production of value-added FA from glycerol electrolysis. *Int. J. Hydrogen Energy* **88**:190–198. DOI:10.1016/j.ijhydene.2024.09.047
132. Zhang J., Shen Y. and Li H. (2023). Electrolysis of glycerol by non-noble metal hydroxides and oxides. *ACS Appl. Energy Mater.* **6**:5508–5518. DOI:10.1021/acsaem.3c00590
133. Shi K., Si D., Teng X., et al. (2023). Enhanced electrocatalytic glycerol oxidation on $CuCoN_{0.6}$/CP at significantly reduced potentials. *Chin. J. Catal.* **53**:143-152. DOI:10.1016/S1872-2067(23)64515-2.
134. Manna B. K., Samanta R. and Barman S. (2024). Porous cobalt–nickel binary oxide nanosheets for electrochemical glycerol oxidation. *ACS Appl. Energy Mater.* **7**:11787–11798. DOI:10.1021/acsaem.4c01995
135. Deng X., Li M., Fan Y., et al. (2020). Constructing multifunctional 'Nanoplatelet-on-Nanoarray' electrocatalyst with unprecedented activity towards novel selective organic oxidation reactions to boost hydrogen production. *Appl. Catal. B Environ.* **278**:119339. DOI:10.1016/j.apcatb.2020.119339
136. Andreu T., Mallafré M., Molera M., et al. (2022). Effect of thermal treatment on nickel - cobalt electrocatalysts for glycerol oxidation. *ChemElectroChem* **9**:e202200100. DOI:10.1002/celc.202200100
137. Fan L., Ji Y., Wang G., et al. (2022). High entropy alloy electrocatalytic electrode toward alkaline glycerol valorization coupling with acidic hydrogen production. *J. Am. Chem. Soc.* **144**:7224–7235. DOI:10.1021/jacs.1c13740
138. Zhang Q., Zhang G., Guan S., et al. (2024). N-CoFeP/NF electrocatalyst for coupling hydrogen production and oxidation reaction of various alcohols. *J. Colloid Interface Sci.* **662**:686–694. DOI:10.1016/j.jcis.2024.02.092
139. Li Y., Wei X., Chen L., et al. (2019). Nickel-molybdenum nitride nanoplate electrocatalysts for concurrent electrolytic hydrogen and FA productions. *Nat. Commun.* **10**:5335. DOI:10.1038/s41467-019-13375-z
140. Mürtz S. D., Musialek F., Pfänder N., et al. (2023). Bimetallic PtCu/C catalysts for glycerol assisted hydrogen evolution in acidic media. *ChemElectroChem* **10**:e202201114. DOI:10.1002/celc.202201114
141. Xu C., Tian Z., Shen P., et al. (2008). Oxide (CeO_2, NiO, Co_3O_4 and Mn_3O_4)-promoted Pd/C electrocatalysts for alcohol electrooxidation in alkaline media. *Electrochim. Acta* **53**:2610–2618. DOI:10.1016/j.electacta.2007.10.036
142. Su Y., Xu Q., Zhong Q., et al. (2015). Oxide (Co_3O_4, NiO, Mn_3O_4, MgO) promoted Au/C catalyst for glycerol electrooxidation in alkaline medium. *Mater. Res. Bull.* **64**:301–305. DOI:10.1016/j.materresbull.2015.01.007
143. Liu Y., Peng R., Xu Y., et al. (2025). Activating glycerol deep oxidation via Au–TiO_x interfacial synergy in bimetallic nanocatalysts. *J. Mater. Chem. A* **13**:36403–36412. DOI:10.1039/d5ta06420a
144. Zanata C. R., Fernández P. S., Troiani H. E., et al. (2016). Rh-decorated PtIrO nanoparticles for glycerol electrooxidation: Searching for a stable and active catalyst. *Appl. Catal. B Environ.* **181**:445–455. DOI:10.1016/j.apcatb.2015.08.021
145. Guo Y., Xu Y. and Chen P. (2025). Ampere-level glycerol electrooxidation enabled by oxygen vacancy-riched crystalline/amorphous Co_3O_{4-x}/ZrO_{2-x} Heterointerface. *J. Colloid Interface Sci.* **699**:138292. DOI:10.1016/j.jcis.2025.138292
146. Li C., Li H., Zhang B., et al. (2024). Efficient electrocatalytic oxidation of glycerol to FA coupled with nitrate reduction over Cu-doped NiCo alloy supported on nickel foam. *Angew. Chem. Int. Ed.* **63**:e202411542. DOI:10.1002/anie.202411542
147. Bai J., Huang H., Li F-M., et al. (2019). Glycerol oxidation assisted electrocatalytic nitrogen reduction: ammonia and glyceraldehyde co-production on bimetallic RhCu ultrathin nanoflake nanoaggregates. *J. Mater. Chem. A* **7**:21149–21156. DOI:10.1039/C9TA08806G
148. Tran G. S., Vo T. G. and Chiang C. Y. (2023). Operando revealing the crystal phase transformation and electrocatalytic activity correlation of MnO_2 toward glycerol electrooxidation. *ACS Appl. Mater. Interfaces* **15**:22662–22671. DOI:10.1021/acsami.3c00857
149. Zhong S., He B., Wei S., et al. (2025). Dynamic Fe-O-Cu induced electronic structure modulation on CuO electrode for selective electrocatalytic oxidation of glycerol. *Appl. Catal. B Environ.* **362**:124743. DOI:10.1016/j.apcatb.2024.124743
150. Ma J., Wang X., Song J., et al. (2024). Synergistic Lewis and Bronsted acid sites promote OH^* formation and enhance FA selectivity: towards high-efficiency glycerol valorization. *Angew. Chem. Int. Ed.* **63**:e202319153. DOI:10.1002/anie.202319153
151. Luo W., Tian H., Li Q., et al. (2023). Controllable electron distribution reconstruction of spinel $NiCo_2O_4$ boosting glycerol oxidation at elevated current density. *Adv. Funct. Mater.* **34**:2306995. DOI:10.1002/adfm.202306995
152. Boukil R., Tuleushova N., Cot D., et al. (2020). Enhanced electrocatalytic activity and selectivity of glycerol oxidation triggered by nanoalloyed silver-gold nanocages directly grown on gas diffusion electrodes. *J. Mater. Chem. A* **8**:8848–8856. DOI:10.1039/D0TA01063D

FUNDING AND ACKNOWLEDGMENTS

This review was supported by National Natural Science Foundation of China (52572330, 52271232) and Ningbo Youth Science and Technology Leading Talents Project (2023QL026). The funders had no role in study design, data collection and analysis, decision to publish, or preparation of the manuscript.

AUTHOR CONTRIBUTIONS

S.B. Wang and H.C. Li wrote the draft. S.B. Wang and Y.C. Lin edited and revised the manuscript. Z.Y. Ma revised the manuscript. L. Chen and Y.C. Lin supervised the manuscript. All authors contributed to the manuscript and approved the final version.

DECLARATION OF INTERESTS

The authors declare no competing interests. The funders had no role in study design, data collection and analysis, decision to publish, or preparation of the manuscript

DATA AND CODE AVAILABILITY

No new data were created or analyzed in this study.